QUADRATURE-POINT STABILIZATION OF MACH-ZEHNDER INTERFEROMETERS

by

RAJESH RAMCHANDER

THESIS submitted to the Faculty of the

Virginia Polytechnic Institute and State University

in partial fulfillment of the requirements for the degree of

MASTER OF SCIENCE

in

ELECTRICAL ENGINEERING

APPROVED:

Richard C. Claus

R. O. CLAUS, Chairman

T. C. POON

R. J. Pieper

R. J. PIEPER

January 12, 1990

Blacksburg, Virginia

c.2

LD
5655
V855
1990
R354
c. 2

QUADRATURE-POINT STABILIZATION OF MACH-ZEHNDER INTERFEROMETERS

by

RAJESH RAMCHANDER

R. O. CLAUS, Chairman

ELECTRICAL ENGINEERING

(ABSTRACT)

Optical fiber magnetometers are extremely sensitive devices which are capable of competing with magnetometers implemented using other technologies. Demodulation of the signals detected using these magnetometers can be performed using either homodyne or heterodyne techniques. Higher sensitivities have been achieved using homodyne rather than heterodyne techniques, but with homodyne demodulation there exists the inherent problem of quadrature-point stabilization. Presented here is a review of existing quadrature-point stabilization methods and experimental results concerning the application of one of them which uses a piezoelectric transducer in the reference arm of an all-fiber Mach-Zehnder interferometer.

Acknowledgements

I would like to express my sincere appreciation to my Committee Chairman, Dr. R. O. Claus, for his guidance and assistance during the course of this research. A sincere note of thanks is also extended to the other members of my advisory committee, Dr. T. C. Poon and Dr. R. J. Pieper.

The help from the American Research Corporation of Virginia who sponsored this project is gratefully appreciated and so is all the help extended by everyone at FEORC, people who make working at FEORC an extremely pleasurable experience.

A special note of thanks to Joe Wiencko and Navid Nader for their constant support, guidance and friendship.

Finally, I would like to thank my parents for the love, encouragement, confidence and financial support they provided me throughout my education.

This thesis is dedicated to my parents.

Table of Contents

1.0 INTRODUCTION 1

2.0 OVERVIEW OF THE MACH-ZEHNDER INTERFEROMETER AND ITS APPLICATION IN A MAGNETOMETER 3

2.1 INTRODUCTION 3

2.2 PHASE OR INTERFEROMETRIC SENSORS 4

2.3 MACH-ZEHNDER INTERFEROMETER 5

2.4 MACH-ZEHNDER INTERFEROMETER APPLIED IN A MAGNETOMETER 7

3.0 METHODS OF DEMODULATION 10

3.1 INTRODUCTION 10

3.2 SHORT PATH-DIFFERENCE INTERFEROMETERS 11

3.3 HETERODYNE METHOD 12

3.4 HOMODYNE METHOD 15

3.4.1 ACTIVE METHODS 16

3.4.2 PASSIVE METHODS 17

4.0 QUADRATURE-POINT STABILIZATION TECHNIQUES **20**

4.1 INTRODUCTION 20

4.2 PASSIVE METHODS 22

4.2.1 TWO WAVELENGTH METHOD 24

4.2.2 TWO POLARIZATION METHOD 26

4.2.3 3 X 3 COUPLER METHOD 27

4.3 ACTIVE METHODS 29

4.3.1 EMISSION WAVELENGTH TUNING METHOD 29

4.3.1.1 ELECTROOPTIC TUNING OF SOURCE WAVELENGTH 31

4.3.1.2 TUNING SOURCE WAVELENGTH BY VARYING DIODE LASER DRIVE CURRENT 33

5.0 QUADRATURE-POINT STABILIZATION OF MACH-ZEHNDER INTERFEROMETER USING PZT METHOD **35**

5.1 INTRODUCTION 35

5.2 DESCRIPTION AND WORKING OF THE COMPENSATOR SYSTEM 36

5.3 MODES OF OPERATION 43

5.3.1 LOW GAIN MODE 43

5.3.2 HIGH GAIN MODE 44

5.4 RESULTS AND DISCUSSION 46

6.0 CLOSING REMARKS **54**

6.1 SUMMARY 54

Appendix A. FRINGE PATTERN **56**

A.1 PROGRAM TO GENERATE FRINGE PATTERN 57

Appendix B. BAND PASS FILTER **63**

BIBLIOGRAPHY 66

Vita 68

List of Illustrations

Figure 1. ALL-FIBER MACH-ZEHNDER INTERFEROMETER [2] 6

Figure 2. MAGNETIC RESPONSE CURVES OF METGLAS [2] 9

Figure 3. HETERODYNING MACH-ZEHNDER INTERFEROMETER [1] 13

Figure 4. INTERFEROMETER OUTPUT VERSUS PHASE SHIFT [10] 18

Figure 5. VARIATION OF FREQUENCY SHIFT WITH MODULATION FREQUENCY [9] . . . 34

Figure 6. BLOCK DIAGRAM OF FEEDBACK CIRCUIT 37

Figure 7. CIRCUIT DIAGRAM OF FEEDBACK CIRCUIT 38

Figure 8. CIRCUIT DIAGRAM OF A LOW PASS FILTER OR INTEGRATOR 40

Figure 9. BODE PLOT OF A LOW PASS FILTER OR INTEGRATOR 41

Figure 10. CIRCUIT DIAGRAM OF BAND PASS FILTER [15] 45

Figure 11. MODULATION AT 1 kHz. WITH STABILIZATION 49

Figure 12. MODULATION AT 10 Hz. WITHOUT STABILIZATION 50

Figure 13. MODULATION AT 10 Hz. WITH STABILIZATION 51

Figure 14. FFT OF FEEDBACK SIGNAL WITHOUT MODULATION 52

Figure 15. FFT OF FEEDBACK SIGNAL WITH MODULATION 53

Figure 16. OUTPUT VERSUS PHASE DIFFERENCE (MAX = 0 RAD) 58

Figure 17. OUTPUT VERSUS PHASE DIFFERENCE (MAX = 2 RAD) 59

Figure 18. OUTPUT VERSUS PHASE DIFFERENCE (MAX = 3.14 RAD) 60

Figure 19. OUTPUT VERSUS PHASE DIFFERENCE (MAX = 5 RAD) 61

Figure 20. OUTPUT VERSUS PHASE DIFFERENCE (MAX = 10 RAD) 62

Figure 21. IDEAL AND PRACTICAL PASS BAND MAGNITUDES [15] 64

1.0 INTRODUCTION

Optical fiber sensor development has matured to the point where these devices have replaced or are on the verge of replacing several existing non-fiber sensors. Fiber sensors offer several advantages over existing technologies: higher sensitivity, geometric versatility, dielectric construction so that they can be used in high electric field, electrically noisy, high temperature, corrosive, or other harsh environments, and compatibility with optical fiber telemetry technology.

The principle on which all optical fiber sensors operates is the modulation of some parameter of the light guided through an optical fiber by an external effect, and the subsequent demodulation of that parameter of light to give an estimate of the external effect. There exist many ways by which guided light may be modulated by an environmental parameter. A constant light source (constant in intensity, frequency, phase, polarization, wavelength or mode) which is launched into an optical fiber can be modulated in one of the above-mentioned constant properties in a certain modulation zone. This modulated light is converted into an intensity modulation, then detected and demodulated to give information about the parameter being sensed. In interferometric sensors the parameter which is modulated is the optical phase.

Chapter 2 introduces the Mach Zehnder interferometer and its application in a magnetometer. Chapter 3 discusses demodulation techniques, projects the homodyne method as more promising and talks about the quadrature point stabilization problem associated with the homodyne demodulation technique. Three passive and two active methods to tackle the signal fading problem are discussed in chapter 4. Chapter 5 finally describes the components of another quadrature point stabilization method, the PZT method, and presents some results obtained on its application to a Mach Zehnder interferometer used as a magnetometer, while chapter 6 summarizes these results. The appendix included at the end facilitates the understanding of some of the results in chapter 5.

2.0 OVERVIEW OF THE MACH-ZEHNDER INTERFEROMETER AND ITS APPLICATION IN A MAGNETOMETER

2.1 INTRODUCTION

The optical fiber interferometer since its first demonstration has proven to be very sensitive and is a prime candidate when extremely small signals have to be measured.

This chapter describes interferometric sensors in general and the Mach-Zehnder interferometer in particular. It then discusses the application of the Mach-Zehnder interferometer in a magnetometer.

2.2 PHASE OR INTERFEROMETRIC SENSORS

In 1801, Thomas Young in his classic two-slit experiment showed that coherent light from two sources could combine to form regions of brightness and darkness called fringes. Young showed that to have a maximum at any point the difference in optical path from the sources to that point must contain an integral number of wavelengths and to have a minimum it must contain an odd number of half wavelengths.

Optical fiber interferometric sensors or interferometers operate on the principle of interference between light carried in the two arms of the interferometer. They detect the phase difference between the two beams. The optical phase in one of the arms is modulated by the parameter of interest resulting in the modulation of the phase difference between the two beams. The modulated phase difference is detected at the output of the interferometer and the external effect is thus sensed. The principal attraction of these devices is their inherent high sensitivity to environmental modulation resulting in extremely high resolution.

Interferometers can be used in a variety of configurations depending on the application. The important configurations are the Mach-Zehnder, Michelson and Fabry-Perot interferometers. The Fabry-Perot interferometer differs from the other two in that it contains only one arm and detects the phase difference between two points on the same arm. Extremely sensitive interferometers in each of the above configurations are capable of detecting phase shifts in the micro-radian range. Optical fiber hydrophones, magnetometers, accelerometers, strain gauges and thermometers have all achieved sensitivities comparable to or exceeding that available from other technologies.

2.3 MACH-ZEHNDER INTERFEROMETER

The configuration of a simple all-fiber Mach-Zehnder interferometer is shown in Fig. 1. Light is launched into two optical fibers from a single source using a 1X2 fiber coupler. One fiber path is the untouched reference arm, the other path is the sensing arm which is exposed to the perturbation of interest. The two arms are recombined using a 2X2 fiber coupler to produce an interference signal at the detectors.

On the photodetector D1, the fields from the two beams add, and the resultant field is given by [1]

$$E_{tot} = E_1 \sin \omega t + E_2 \sin(\omega t + \phi(t)), \tag{2.1}$$

where E_1 is the optical field amplitude in the reference arm, E_2 is that in the sensing arm, and $\phi(t)$ is the time varying difference between the optical phases in the two arms. The interference phenomenon that takes place when the two beams are combined effectively converts the phase modulation to a spatially periodic intensity modulation. The photodetector D1 responds to the intensity of the combined beams, and thus the photodetector current i(t) is

$$i(t) \propto [1 + \cos \phi(t)] \tag{2.2}$$

at the output of detector D1 and proportional to $[1 - \cos \phi(t)]$ at the output of detector D2, for the case where the field amplitudes in the two arms are equal.

The response of the detected light intensity to small changes in relative phase between the two arms of the interferometer obtained upon differentiating Eq. 2.2 is

$$\delta i(t) = \sin \phi \delta \phi. \tag{2.3}$$

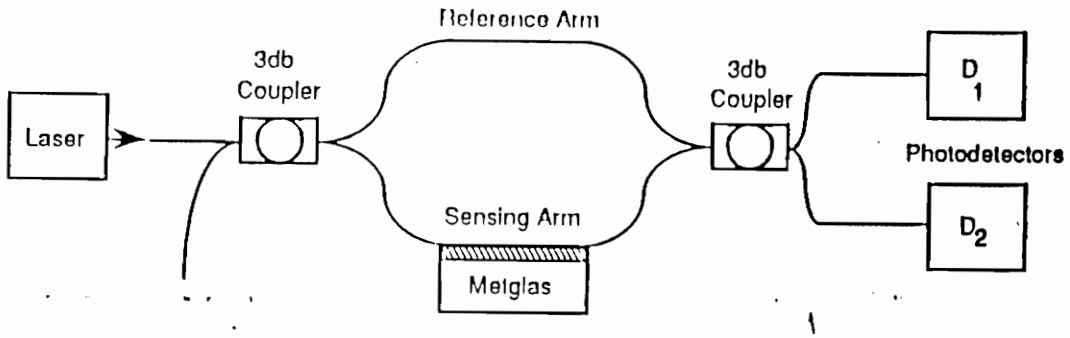

Figure 1. ALL-FIBER MACH-ZEHNDER INTERFEROMETER [2]

Any change in the relative phase is translated into a change in the current in the detectors. The Mach-Zehnder interferometer is thus used to detect optical phase shifts between the optical fields propagating in its two arms. The optical phase in the sensing arm is modulated by the parameter of interest. This results in the indirect modulation of the phase difference between the two beams. Since the Mach-Zehnder interferometer can detect the optical phase difference between its two arms, in effect, the external parameter is being detected.

2.4 MACH-ZEHNDER INTERFEROMETER APPLIED IN A MAGNETOMETER

Magnetostriction-based sensors rely on a fiber interferometer to measure the change in length of a material resulting from an external magnetic field. This property wherein the dimensions of a ferro-magnetic material are changed upon the application of a magnetic field is termed magnetostriction and is present in all ferro-magnetic materials to varying degrees. Metallic glass (metglas) ribbons exhibit a high degree of magnetostriction, i.e. the change in dimensions of these ribbons is considerable in the presence of a magnetic field. Though initially nickel cylinders were used as the magnetostrictive elements, current research is directed toward metglas because of its superior response.

The length of a metallic glass ribbon is modulated by an external magnetic field and this change in length is coupled to the sensing arm of an all-fiber Mach-Zehnder interferometer by bonding the sensing arm to the metallic glass ribbon. This results in the modulation of phase of the light emerging from the sensing arm which is then demodulated and detected using suitable interferometric techniques to indicate the strength of the external magnetic field [2]. A comparison of various bonding techniques is presented in Ref. 3.

The magnetostrictive response of metglas ($\delta l/l$) follows the coherent rotation model and has a quadratic dependence on the total applied magnetic field H [4], namely,

$$\frac{\delta l}{l} = CH^2. \tag{2.4}$$

This is illustrated in Fig. 2 from which it can be deduced that the AC magnetostrictive response increases from zero to some maximum value before falling back to zero because of magnetic saturation of the ribbon. So, for high-frequency AC magnetic field measurements a DC bias field is applied for operation in the region of maximum sensitivity.

For DC and low-frequency AC magnetic field measurements, a technique which utilizes the dependence between the AC responsitivity and the bias field to detect small changes in the bias field is used [5]. This detection scheme uses a magnetic 'calibration' signal and, in principle, eliminates the problems associated with low-frequency random phase shifts in the interferometer.

Finally, the DC or low-frequency magnetometer can be operated in open or closed-loop configurations. In the open-loop configuration the amplitude of the phase shift is monitored as a function of time to detect changes in the magnetic field. In the closed-loop format, the dynamic magnetostrictive responsitivity of the active sensing element is maintained at zero by the control of the total bias field using current feedback to the biasing coil [6]. The feedback current is now used as a measure of the magnetic field. This ensures that the system is less susceptible to drift and noise associated with the stability of the magnetic 'calibration' signal, resulting in a much larger dynamic range and eliminating problems arising because of hysteresis effects in the active magnetostrictive sensing element.

For a comprehensive review of various stages in the development of magnetic field sensors the reader is referred to Ref. 7.

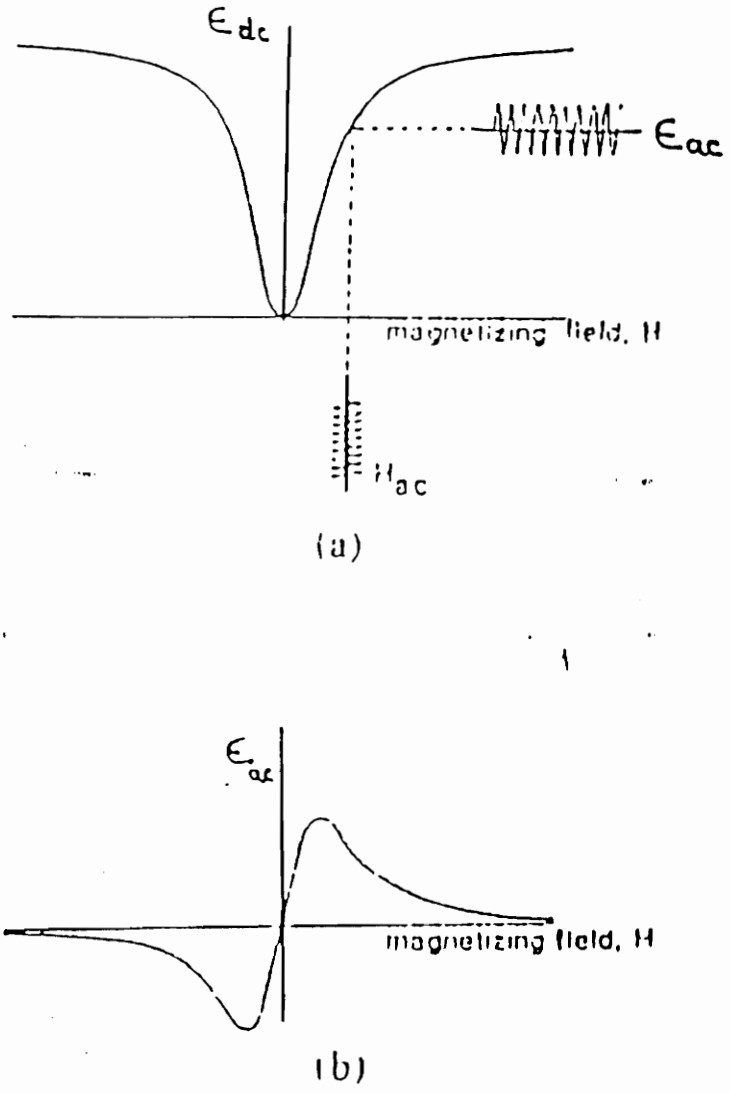

Figure 2. MAGNETIC RESPONSE CURVES OF METGLAS [2]

3.0 METHODS OF DEMODULATION

3.1 INTRODUCTION

The Mach-Zehnder interferometer detects the optical phase difference between its two arms by responding to the intensity variation brought about by the interference phenomenon. Several demodulation schemes to recover information about the phase shift, which is directly related to the parameter being sensed, exist. Each has its own advantages and disadvantages and the selection of a particular scheme depends on many factors like the frequency of the parameter of interest and other noise perturbations, the sensitivity required, and similar factors.

Interferometers usually display high sensitivity to other noise perturbations such as temperature, air currents and acoustic noises in addition to the perturbation of interest. This inherent sensitivity results in the production of a differential drift in the arms of the interferometer. This drift causes changes in the amplitude of the detected signal (signal fading), which under certain circumstances may even be zero. Besides, the signal may also be distorted (frequency up-conversion).

The various demodulation schemes which exist overcome the problems caused by noise perturbations by using different techniques. They include the heterodyne, homodyne (active and passive), synthetic heterodyne, quadrature recombination and variations of these. This chapter describes the first two of the above mentioned techniques and also gives an introduction to the various methods which can be used to maintain the interferometer at quadrature (maximum sensitivity) when used in the homodyne configuration. But first, a condition necessary for the reduction of noise in interferometers, short path-difference, is touched upon. An understanding of this section is necessary to comprehend some considerations made in chapter 4.

3.2 SHORT PATH-DIFFERENCE INTERFEROMETERS

As has been described in the previous chapter, the Mach-Zehnder interferometer has two arms, the sensing arm and the reference arm, and it can detect the phase difference between them. There are some problems associated with interferometers with large path length differences. These complications arise because of the presence of phase noise in the source and its frequency instability.

In all finite path-difference interferometers the effect of optical phase is critical, since the path difference produces the proper condition for conversion of phase noise into amplitude noise. Suppose that the source output is written as $\cos(\omega t + \phi_n(t))$, where $\phi_n(t)$ represents a phase noise term. The two interfering beams then bear phase noise differences $\phi_n(t) - \phi_n(t-\tau)$, where τ is the time during which light undergoes a change of phase ϕ, the mean optical phase difference. The output of the interferometer now is

$$1 + \cos(\phi_n(t) - \phi_n(t-\tau) + \phi). \tag{3.1}$$

If the phase noise function cannot be filtered out, conversion of phase noise to intensity noise may produce significant increases in background noise levels, which increase with increasing path difference.

The other problem concerns the frequency (or wavelength) stability of the source, even in nominally zero path-difference interferometers. Even a fractional change in the operating wavelength of the source can result in the change of a number of wavelengths because of the imbalance in the arms. So, for reasons described above, short (preferably zero) path-difference interferometers are preferred.

3.3 HETERODYNE METHOD

In the heterodyne approach, light in one of the arms of the interferometer is frequency shifted by passing it through a suitable modulator such as a Bragg cell [1]. As shown in Fig. 3 the Bragg cell imposes a frequency shift of ω_B on the optical signal transmitted in the sensing arm relative to that transmitted in the reference arm. The parameter being sensed appears as a frequency modulation (FM) on a carrier at a frequency equal to the difference frequency between the two beams. For the case of equal amplitudes in the two arms the output from the detector is

$$1 + \cos(2\omega_B t + \phi(t)), \tag{3.2}$$

where $\phi(t)$ is the difference in phase between the two arms.

If the parameter of interest which modulates the sensing arm occurs at a frequency away from the frequency at which an environmental perturbation modulates either of the arms, the two

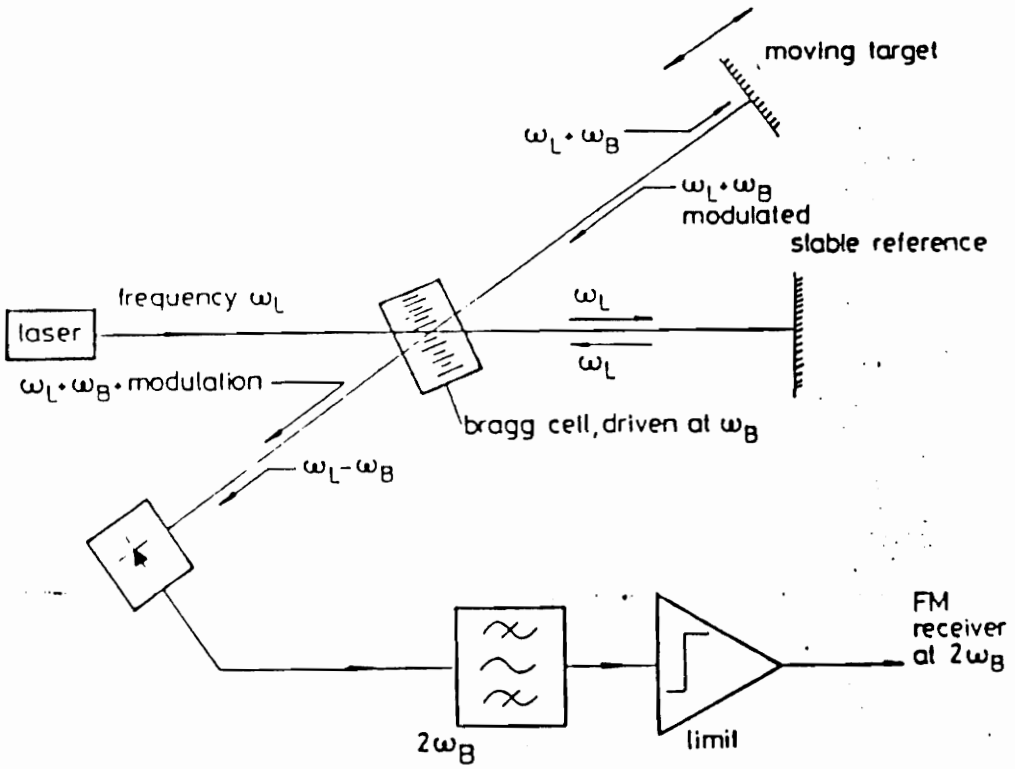

Figure 3. HETERODYNING MACH-ZEHNDER INTERFEROMETER [1]

effects can be separated. This helps in eliminating the signal fading problem. Temperature and air current drifts have been known to occur only at low frequencies. However, environmental acoustic perturbations occur at higher frequencies. If the frequency of the parameter being sensed does not fall into either of the above categories the heterodyne method is very attractive.

Besides, there exist two added advantages with the heterodyne approach. One of them pertains to the detector while the other concerns the source. Semiconductor detectors, while being the most commonly used, have a considerable amount of 1/f noise, especially, of course, at lower frequencies. Since in this approach a part of the incident power is up-shifted to the frequency $2\omega_B$, and because this frequency is well outside the 1/f noise region, there is a considerable improvement in the signal to noise (SNR). Finally, changes in source intensity manifest themselves as optical phase noise. Since the heterodyne method is electronically limited during the detection process, the effects of intensity noise in the source translate into a reduction in the SNR rather than affecting the interferometer reading.

Even though it may seem that the heterodyne method is very attractive, there exists a prominent disadvantage: it is fundamentally impossible to incorporate a conventional frequency shifter like a Bragg cell into an all-fiber form without breaking the fiber and thus introducing mechanically sensitive interfaces. This one difficulty and the fact that smaller phase shifts have been detected by homodyne rather than heterodyne techniques has resulted in homodyne techniques being preferred over heterodyne ones for the application of the Mach-Zehnder interferometer as a magnetometer.

3.4 HOMODYNE METHOD

In the homodyne approach, the light in both arms of the interferometer is at the same frequency. As has been stated in chapter 2, and repeated here for convenience, the response of the detected light intensity to small changes in relative phase between the two arms may be obtained by differentiating Eq. 2.2 to obtain

$$\delta i(t) = \sin \phi \delta \phi. \tag{3.3}$$

Thus, the detected change depends on both the initial phase setting of the interferometer as well as the change in phase. Since the change in phase is the item of interest, it may be conveniently extracted if

$$\sin \phi = 1. \tag{3.4}$$

The condition stated in Eq. 3.4 implies that the relative phases of the two arms of the interferometer be in quadrature; this is called the 'quadrature condition'. When biased at quadrature point, the relationship between the incremental phase change and the incremental intensity change is linear. The linearity is within 1% over a range of 9°, within 2% up to 12°, and within 10% up to 25° relative phase change [1]. An interferometer at quadrature allows an optimized way to extract relative phase changes between its arms.

There exist two principal difficulties with the homodyne arrangement. The output reading of the interferometer is sensitive to the optical power entering the interferometer as well as the relative optical phase at the detector. A 2% drift in the source intensity produces exactly the same effect as somewhat more than 1° phase change [1]. Source stability is thus critical, though only in the bandwidth of the modulation applied to the interferometer. At other frequencies an intensity variation produces a change in the interferometer scale factor. Often these drifts can be reduced with appropriate filtering techniques.

The other main difficulty with this type of arrangement, and which is specifically the topic of this thesis, pertains to keeping the interferometer at quadrature. Maintaining the interferometer at a stable quadrature bias point is far from trivial, unless the interferometer itself is self-compensated in some way (an example would be the Sagnac interferometer). If the interferometer is initially set at quadrature there is a tendency for it to drift away from it. This movement away from quadrature occurs because of the inherent sensitivity of the interferometer to environmental perturbations like temperature and air currents. Temperature fluctuations due to the coefficient of thermal expansion of glass waveguides are an especially serious problem. So quadrature stabilization techniques have to be applied to maintain the interferometer at maximum sensitivity.

Quadrature stabilization can be enforced by active or passive methods. The main difference between an active and passive method are the different optics and electronics required.

3.4.1 ACTIVE METHODS

In an actively stabilized system, the fiber interferometer is kept at its quadrature point for maximum sensitivity by some feedback compensation. Two active compensation schemes with comparable performances have been reported [8, 9]. Both schemes make use of feeding the interferometer output back, either to a piezo-electric transducer (PZT) element [8], or to the current source powering the laser diode [9]. In the case involving the PZT element, the fiber in the reference arm of the Mach-Zehnder interferometer is bonded to the PZT and thus is length-modulated by the interferometer output. As a result, the interferometer is forced to stay at its maximum sensitivity state (quadrature point). The output is extracted from the feedback signal when used in the high gain mode (see chapter 5).

In the case involving current feedback to the laser diode, the optical output is used to modulate the driving current to the laser diode resulting in frequency or wavelength modulation of the laser diode. Source wavelength change effectively is equivalent to path length change in the fiber interferometer. Thus, the result of this stabilization scheme is the same as that with the PZT tracker.

The above stated active stabilization methods have been comprehensively covered in chapters 4 and 5. Minimum detectable phase shifts in actively stabilized systems are in the micro-radian range.

3.4.2 PASSIVE METHODS

In a passively stabilized system, the fiber interferometer is free running with no feedback compensation. The reason that a normal fiber interferometer has signal fading is because a 2X2 fiber coupler provides two light outputs which are at a phase difference of π radians as shown in Fig. 4. The two traces shown here are the interferometer arm intensities as a function of the interferometer differential phase shifts. The detected phase signal is a small perturbation at some point along these traces. When the differential phase shifts of the interferometer are multiples of π radians, both the interferometer outputs have almost zero sensitivity to any phase perturbation. In a passively stabilized system, two optical outputs which are not π radians apart are derived. A 3X3 fiber coupler, for example, provides two outputs which are $\pi/2$ radians apart [10]. Thus, at any instant of time there is no total fading of both the interferometer outputs.

There exist other passive stabilization schemes in addition to the one using a 3X3 coupler and they have been covered in chapter 4. Although the passive stabilization schemes require no

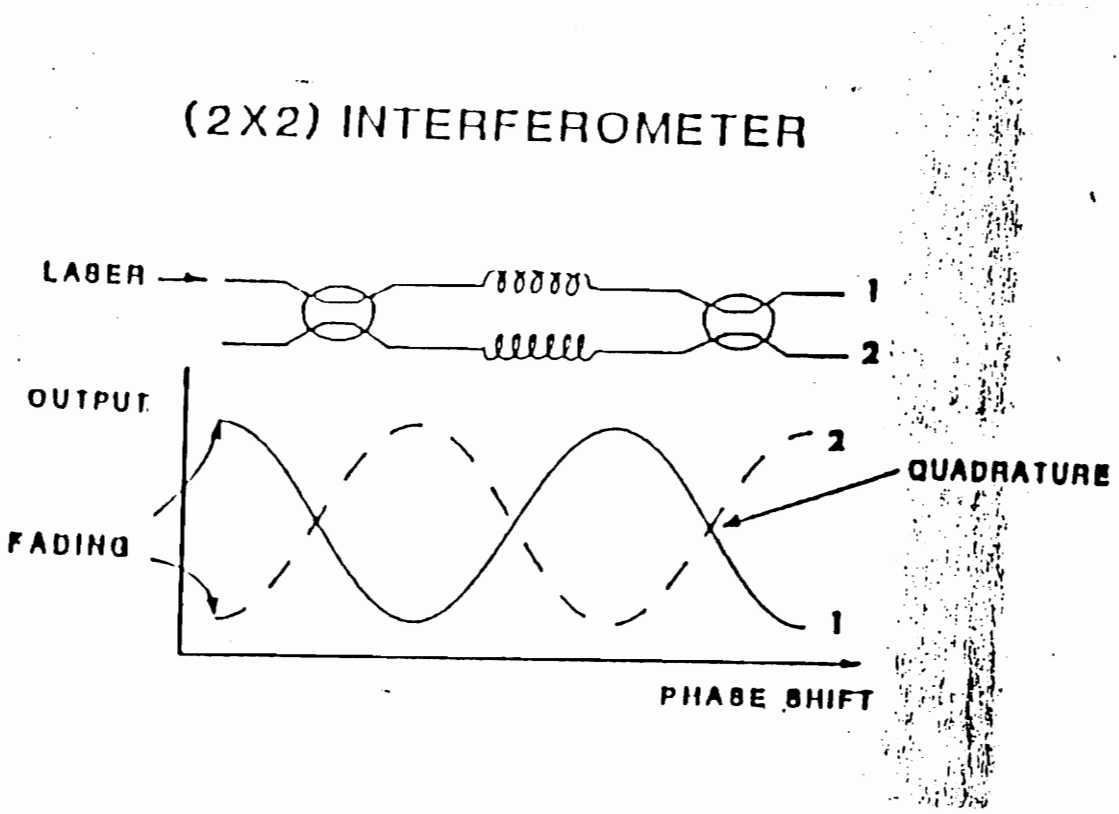

Figure 4. INTERFEROMETER OUTPUT VERSUS PHASE SHIFT [10]

feedback, they need some signal processing to extract a stable undistorted output proportional to the input modulation.

4.0 QUADRATURE-POINT STABILIZATION TECHNIQUES

4.1 INTRODUCTION

As stated in previous chapter, the homodyne method, though more sensitive than the heterodyne method, requires some sort of quadrature point stabilization to maintain the interferometer at maximum sensitivity. There exist both active and passive methods to do just this. Active methods utilize some sort of feedback compensation while passive ones are free-running with no feedback.

If P_{in} is the optical input into the Mach-Zehnder interferometer shown in Fig. 1, it is equally divided into two beams by coupler 1. These two beams propagate along the two single-mode fibers arms and are recombined at coupler 2. Assuming a unit input $P_{in} = 1$, the outputs P_1 and P_2 of coupler 2 can be expressed as

$$P_1 = \frac{1}{2}(1 + \cos \phi), \tag{4.1}$$

$$P_2 = \frac{1}{2}(1 - \cos \phi), \tag{4.2}$$

$$\phi = -\frac{2\pi S n_{eff}(\lambda)}{\lambda}, \tag{4.3}$$

where $n_{eff}(\lambda)$ is the effective refractive index of the guided mode in the fiber, λ is the wavelength, and S and ϕ are the path length and phase difference between the two arms.

Both S and ϕ are time varying quantities which are being sensed by the interferometer and which are dependent on the external parameter which varies them. In fact, the external parameter actually varies S, while the variation in ϕ is the result of the interference phenomenon at coupler 2. The signal to be detected thus induces a change in ϕ which in turn induces a change in P_1 and P_2. The change in P_1 due to the change in ϕ obtained on differentiating Eq. 4.1 is

$$\delta P_1 = -\frac{1}{2}\delta\phi \sin \phi. \tag{4.4}$$

Thus, for a given signal $\delta\phi$, the output change $\delta P_1 (= -\delta P_2)$ is proportional to sin ϕ.

Environmental temperature and air pressure perturbations are capable of fluctuating ϕ over many radians. It is possible to detect a small signal only when the temporal frequency of $\delta\phi$ is well outside the frequency spectrum of the environmental noises. Even here, the output signal δP_1 suffers from fading whenever sin ϕ becomes equal to zero. The rest of this chapter and the next discusses methods to avoid signal fading and thus maintain the interferometer at quadrature by using active and passive stabilization techniques.

4.2 PASSIVE METHODS

In passive schemes two outputs which are out of phase by $\pi/2$ radians are generated. The outputs of two detectors which are out of phase by $\pi/2$ radians can be expressed as

$$P_1 = A_1 + A_2 \cos \phi \tag{4.5(a)}$$

$$P_2 = B_1 + B_2 \sin \phi \tag{4.5(b)}$$

where A_1, A_2, B_1 and B_2 are constants and $\phi(t)$ is the optical phase difference between the sensing and the reference arms. On removal of the dc offsets the two detector outputs can now be represented by

$$P_1 = A \cos \phi \tag{4.6(a)}$$

$$P_2 = B \sin \phi \tag{4.6(b)}$$

where A and B are constants.

The change in the detector outputs for small changes in the phase between the two arms obtained by differentiating Eq. 4.6 is

$$\delta P_1 = - A\delta\phi \sin \phi \tag{4.7(a)}$$

$$\delta P_2 = B\delta\phi \cos \phi. \tag{4.7(b)}$$

A number of signal processing techniques can now be applied to avoid signal fading and to recover a reasonable signal. Four simple schemes described by Eqs. 4.8, 4.9, 4.10 and 4.11 follow.

$$\delta P = \frac{P_1(\delta P_2) - P_2(\delta P_1)}{AB\delta\phi(\cos^2\phi + \sin^2\phi)}, \qquad (4.8(a))$$

which on integration gives

$$P = AB\phi. \qquad (4.8(b))$$

Another scheme could be

$$\delta P = \frac{-B(\delta P_1) + A(\delta P_2)}{AB(\sin\phi + \cos\phi)\delta\phi}, \qquad (4.9(a))$$

which on normalization could yield

$$\frac{\delta P}{BP_1 + AP_2} = \delta\phi. \qquad (4.9(b))$$

Eq. 4.9(b) then could be integrated to achieve

$$P = \int \frac{\delta P}{BP_1 + AP_2} = \phi. \qquad (4.9(c))$$

A third processing scheme could be

$$\delta P = \frac{(B^2(\delta P_1)^2 + A^2(\delta P_2)^2)^{1/2}}{AB\delta\phi}. \qquad (4.10(a))$$

This could again be integrated as in Eq. 4.8(b) to yield

$$P = AB\phi. \qquad (4.10(b))$$

A final and simple scheme could be

$$\delta P = \max(|B\delta P_1|, |A\delta P_2|), \qquad (4.11)$$

which could be normalized by taking either $\frac{\delta P}{AP_2}$ or $\frac{\delta P}{BP_1}$. Finally, $\frac{\delta P}{AP_2}$ or $\frac{\delta P}{BP_1}$ could be integrated to obtain an output proportional to ϕ.

The electronic manipulation such as addition, multiplication, squaring and square rooting in the first three methods described by Eqs. 4.8, 4.9 and 4.10 may induce extra noise thus imposing a limit on the minimum detectable signal level. However the level of the minimum detectable signal would not be affected in the final scheme as normalization is done after the output changes are detected. The next three sections indicate methods by which the $\pi/2$ radian phase difference between the two detector outputs can be generated.

4.2.1 TWO WAVELENGTH METHOD

From Eq. 4.3 it can be seen that the relative phase of light between the two arms of the Mach-Zehnder interferometer is dependent on the wavelength of light. Since the outputs at the detectors depend on the phase difference between the arms as is evident from Eq. 4.1 and 4.2, the interferometer can be held at quadrature by controlling the wavelength of light.

If the input P_{in} ($= 1$) is composed of or equivalently switched between two wavelengths λ_1 and λ_2 such that [11]

$$\phi(\lambda_2) - \phi(\lambda_1) = \frac{\pi}{2}, \tag{4.12}$$

the interferometer can be maintained at quadrature as explained. Eq. 4.12 can be satisfied if the following conditions are met:

$$\phi(\lambda_1) = 2m\pi, \tag{4.13(a)}$$

and

$$\phi(\lambda_2) = 2m\pi + \frac{\pi}{2}, \qquad (4.13(b))$$

where m is any real number.

Substituting Eq. 4.13 into 4.1 and 4.2 the following results can be obtained.

$$P_1(\lambda_1) = \frac{1}{2}(1 + \cos\phi), \qquad (4.14(a))$$

and

$$P_2(\lambda_2) = \frac{1}{2}(1 + \sin\phi). \qquad (4.14(b))$$

Since Eq. 4.14 resembles Eq. 4.5 exactly, any of the four signal processing schemes can be used to maintain the interferometer at quadrature thus extracting a reasonably stable signal.

A necessary condition for this set-up to function properly is that 'm' in Eq. 4.13 should be large enough so that either the signal being sensed or environmental noise does not produce a path-length difference twice that of the initial setting. If environmental noise does produce a path-length difference twice that of the initial difference Eq. 4.13 becomes

$$\phi(\lambda_1) = 4m\pi, \qquad (4.15(a))$$

$$\phi(\lambda_2) = 4m\pi + \pi. \qquad (4.15(b))$$

This implies that the two detector outputs have a phase difference of π radians instead of the required phase difference of $\pi/2$ radians.

However, this is in direct contradiction to having short path difference between the interferometer arms described in section 3.2 to reduce the amount of noise at the output. So

a reasonable compromise between the maintenance of quadrature and an increase in system noise has to be determined.

4.2.2 TWO POLARIZATION METHOD

Theoretically, doubly degenerate HE_{11} modes are supported by single-mode fibers with perfectly round cross-sections. The HE_{11} modes of two orthogonal polarizations are degenerate in this case. However, in reality, internal strains and non-perfect cross-sections remove the degeneracy and introduce a certain degree of birefringence. Commercially available single-mode fibers have a beat-length (L_p) in the range of 0.1-10 m [11]. Beat-length can be defined by

$$L_p = \frac{\lambda}{n_1 - n_2}; \tag{4.16}$$

where n_1 and n_2 are the effective indices of refraction of the two orthogonally polarized guided modes. In birefringent fibers the beat-length may be as small as a few millimeters [11]. Let the two orthogonal polarizations be p and s and assume that the input light excites both polarizations equally.

If the condition

$$|\phi(p) - \phi(s)| = |-2\pi S \frac{(n_1 - n_2)}{\lambda}| = \frac{\pi}{2} \tag{4.17}$$

is satisfied then on substituting Eq. 4.17 into 4.1 and 4.2

$$P_1(\lambda_1) = \frac{1}{2}(1 + \cos\phi), \tag{4.18(a)}$$

and

$$P_2(\lambda_2) = \frac{1}{2}(1 + \sin\phi), \tag{4.18(b)}$$

can be obtained. The condition in Eq. 4.17 can be obtained if

$$S = \frac{L_p}{4}. \tag{4.19}$$

The same results as those achieved using the two wavelength approach is thus obtained. So any of the four signal processing methods described by Eqs. 4.8, 4.9, 4.10 or 4.11 can be used to get a reasonably stable output signal which is proportional to the phase shift.

4.2.3 3 X 3 COUPLER METHOD

This is probably the most popular passive quadrature stabilization method as it puts no demands on the source but rather on the signal processing at the output. Reducing the restrictions on the optical source reduces the cost of implementing this method compared to the two wavelength approach.

The key element in this approach is the use of a 3X3 directional coupler as the beam combiner in the fiber interferometer instead of the 2X2 fiber coupler employed in other methods. The three interferometer outputs are given by [10]

$$P_I = -2B_2(1 + \cos\phi), \tag{4.20(a)}$$

$$P_{II} = B_1 + B_2\cos\phi + B_3\sin\phi, \tag{4.20(b)}$$

and

$$P_{III} = B_1 + B_2\cos\phi - B_3\sin\phi, \tag{4.20(c)}$$

where B_i (i = 1, 2, 3) are constants which depend on the coupling coefficients of the coupler and $\phi(t)$ is the differential phase shift of the interferometer.

On processing P_{II} and P_{III} in the following manner the required phase difference of $\pi/2$ radians can be readily obtained.

$$P_A = \frac{P_{II} + P_{III}}{2(B_1 + B_2 \cos \phi)} \tag{4.21(a)}$$

$$P_B = \frac{P_{II} - P_{III}}{2B_3 \sin \phi.} \tag{4.21(b)}$$

With the differential cross-multiplication one can obtain

$$D = \frac{P_A \frac{dP_B}{dt} - P_B \frac{dP_A}{dt}}{4B_1B_3 \frac{d\phi}{dt} \cos \phi + 4B_2B_3 \frac{d\phi}{dt}}. \tag{4.22}$$

Eq. 4.22 can be integrated to obtain

$$E = \frac{\int D dt}{4B_1B_3 \sin \phi + 4B_2B_3\phi.} \tag{4.23}$$

Since B_1 is the dc output of P_{II} and P_{III} it can be set to zero by introducing offsets in the processing electronics. This results in

$$E = 4B_2B_3\phi \tag{4.24}$$

which is directly proportional to the interferometers phase shift.

From the above equations it can be seen that distortions will be seen in the output if the electronics is not properly balanced, i.e. if B_1 is not exactly equal to zero. The equations above were derived for a single polarization scheme. In practice, small deviations from the $\pi/2$

radian phase shift between P_{II} and P_{III} will be observed. Eq. 4.24 will therefore have to be multiplied by a factor cos Δ i.e.

$$E = 4B_2B_3 \cos \Delta, \tag{4.25}$$

where Δ is the angular deviation from $\pi/2$ radians, to allow for this effect [11].

4.3 ACTIVE METHODS

Active stabilization schemes keep the interferometer at quadrature by varying the optical path length of the two beams such that $\phi = \pi/2$ radians or $\sin \phi = 1$, where ϕ is the phase difference between the two arms. In the case of the PZT method [8] the length of the reference arm is physically modulated in accordance with the noise perturbation. In the method where the source frequency is tuned [9], the output wavelength of the laser-diode is again varied proportionally to the extraneous perturbation. The effective path length difference due to the variation of source wavelength is maintained at a constant value and the operating point of the interferometer is held at quadrature.

4.3.1 EMISSION WAVELENGTH TUNING METHOD

Emission wavelength tuning is one of the popular methods to maintain a Mach-Zehnder interferometer at quadrature. After a brief description of the theory behind wavelength tuning, two variations, one which involves electooptic tuning of the laser source and the other which pertains to tuning the emission frequency by controlling the drive current of the laser are discussed.

In an interferometer the phase difference ϕ between the two arms may be expressed as

$$\phi = \frac{2\pi x}{\lambda}, \tag{4.26}$$

where x is the optical path difference between the two arms and λ is the wavelength of light. Note that

$$x = nl, \tag{4.27}$$

where n is the refractive index of the medium in which the signals propagate and l is the linear path difference between the two arms of the interferometer. A variation in either x or λ causes a phase shift given by

$$\Delta\phi = \frac{2\pi}{\lambda}(\Delta x - x\frac{\Delta\lambda}{\lambda}). \tag{4.28}$$

It can be easily seen from Eq. 4.28 that any change in phase attributable to optical path length variation may be compensated by a shift in the wavelength of light.

The quadrature condition is given by

$$\phi = 2m\pi + \frac{\pi}{2}, \tag{4.29(a)}$$

or

$$\phi = 2m\pi - \frac{\pi}{2}, \tag{4.29(b)}$$

where m is an integer, while the condition for phase stability for active methods is given by

$$\Delta\phi = 0. \tag{4.30}$$

Substituting Eq 4.30 in 4.28 the condition for phase stability,

$$\Delta\lambda = \frac{\lambda \Delta x}{x}, \tag{4.31}$$

can be readily obtained.

To compensate for a phase change $\phi = 2\pi$ or an optical path length change $\Delta x = \lambda$, the interval over which the wavelength would have to be tuned can be obtained from Eq. 4.31 [12] as

$$(\Delta\lambda)_{2\pi} = \frac{\lambda^2}{x}. \tag{4.32}$$

Eq. 4.32 implies that the required minimum tuning interval $(\Delta\lambda)_{2\pi}$ can be reduced by increasing the optical path length difference x. This path length difference is only limited by the coherence length of the laser. However this increases the phase noise as reported in section 3.2. So, in practice, the path difference is made as small as possible within the available tuning range [12].

With this general introduction two methods where the laser output wavelength is varied is described below. The generation of the error signal which controls the tuning of the wavelength in the first one is also covered. However, as the error signal generation for second method is exactly the same as the one for the PZT method, it is described in the next chapter which covers the PZT method for quadrature point stabilization in detail.

4.3.1.1 ELECTROOPTIC TUNING OF SOURCE WAVELENGTH

As has already been mentioned in Eqs. 4.1 and 4.26 the output of coupler 2 of an interferometer is

$$P = P_0(1 + \cos\phi), \tag{4.33}$$

while the phase difference between its arms is

$$\phi = \frac{2\pi x}{\lambda}. \tag{4.34}$$

Differentiating Eq. 4.34 with respect to λ we can obtain

$$\frac{d\phi}{d\lambda} = -\frac{\phi}{\lambda}. \tag{4.35}$$

The error signal can be taken as the linear combination

$$\Delta V = \frac{d^2P}{d\lambda^2} + \frac{2}{\lambda}\frac{dP}{d\lambda}. \tag{4.36}$$

On equating the error signal to zero the quadrature condition $\phi = \pi/2$ radians is obtained.

This error signal described by Eq. 4.36 can be applied to an electooptic tuner controlling the source wavelength in the form of a voltage. The change in the output wavelength as a function of the error signal is described [13] by

$$\Delta\lambda = C\Delta V, \tag{4.37}$$

where C is the tuning rate of the electrooptic tuner. Substituting Eq. 4.37 into 4.35 the final result,

$$\Delta\phi = -\frac{\phi}{\lambda} C\Delta V, \tag{4.38}$$

is obtained. Eq. 4.38 indicates that any externally induced phase change either by noise alone (low gain) or by the signal and noise together (high gain) will be nulled out by an equal, but of opposite sign, phase change. The low and high gain modes of operation of the interferometer are explained in chapter 5 with respect to the PZT method.

4.3.1.2 TUNING SOURCE WAVELENGTH BY VARYING DIODE LASER DRIVE CURRENT

The method for the generation of the error signal here is exactly the same as the one used in the PZT method. So it is covered in detail in chapter 5 which deals with the PZT method. However, one important fact is mentioned here.

The output wavelength of a laser source can be controlled by the drive current. The change in frequency $\delta\nu$ with current δi, i.e. $\delta\nu/\delta i$ is a function of the modulation frequency as described by Fig. 5 [14]. The current to the diode laser powering the interferometer may be changed so that the effective phase shift produced by variation in the optical path length difference δx and the frequency shift $\delta\nu$ cancel out each other, thus maintaining the interferometer at quadrature.

The change in the laser-diode output frequency $\delta\nu$ necessary to balance an optical path length variation δx is given by [14]

$$\delta\nu = \frac{\delta x}{x}\nu, \tag{4.39}$$

where x is the optical path difference between the arms of the interferometer and ν is the nominal frequency. The signal current δi necessary to produce a frequency shift $\delta\nu$ is given by [14]

$$\delta i = \left(\frac{d\nu}{di}\right)_f^{-1}\delta\nu. \tag{4.40}$$

In Eq. 4.40 the term $\left(\frac{d\nu}{di}\right)_f^{-1}$ is present to indicate the fact that large currents are required to to compensate for optical path-length changes if the modulation frequencies are high.

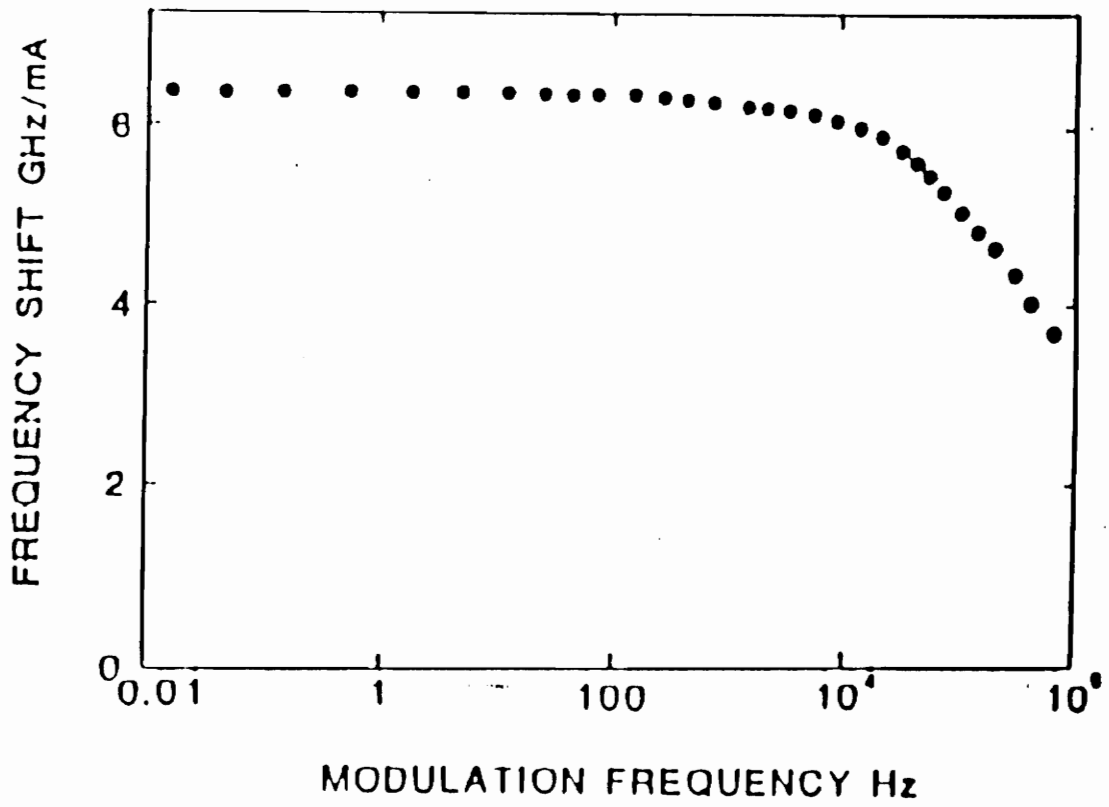

Figure 5. VARIATION OF FREQUENCY SHIFT WITH MODULATION FREQUENCY [9]

5.0 QUADRATURE-POINT STABILIZATION OF MACH-ZEHNDER INTERFEROMETER USING PZT METHOD

5.1 INTRODUCTION

This chapter explains very thoroughly another active stabilization technique which utilizes a piezo electric transducer (PZT) in the reference arm of a Mach-Zehnder interferometer. This chapter is divided into three sections. Section one describes the compensator system which includes the feedback circuit generating the error signal and the PZT itself. It also explains the working of the compensator system. The second part talks about the operation of the interferometer in the low and high gain modes. The final section includes results obtained upon the application of this compensation system on a Mach-Zehnder interferometer configured as a magnetometer and discusses these results.

It should be noted that the error signal generator circuit mentioned in chapter 4 which pertains to source wavelength tuning by varying diode laser drive current is the same as the feedback circuit described below.

5.2 DESCRIPTION AND WORKING OF THE COMPENSATOR SYSTEM

Fig. 6 shows the components present in the feedback circuit in the form of a block diagram [8]. It consists of a differential amplifier, low pass filter, integrator and an inverting amplifier. The circuit diagram of the feedback circuit is shown in Fig. 7 along with the individual components. The IC 741 is used as the active element in all the four blocks.

The inputs to the differential amplifier come from the two detectors of the Mach-Zehnder interferometer. The outputs of the two detector currents when converted to voltages are of the form

$$V_1 = V_A + V_B \cos \phi \qquad (5.1(a))$$

and

$$V_2 = V_A - V_B \cos \phi, \qquad (5.1(b))$$

where V_A and V_B are proportional to the laser power and $\phi(t)$ is the phase difference between the two arms. The ratio V_A/V_B is constant unless the fibers are dynamically twisted. The differential amplifier amplifies the difference between its two inputs depending on the value of the resistors according to

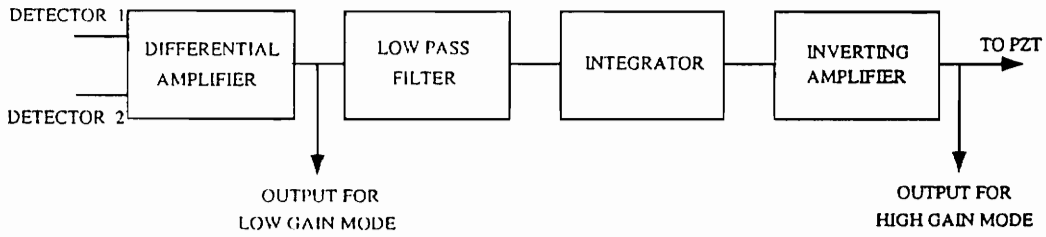

Figure 6. BLOCK DIAGRAM OF FEEDBACK CIRCUIT

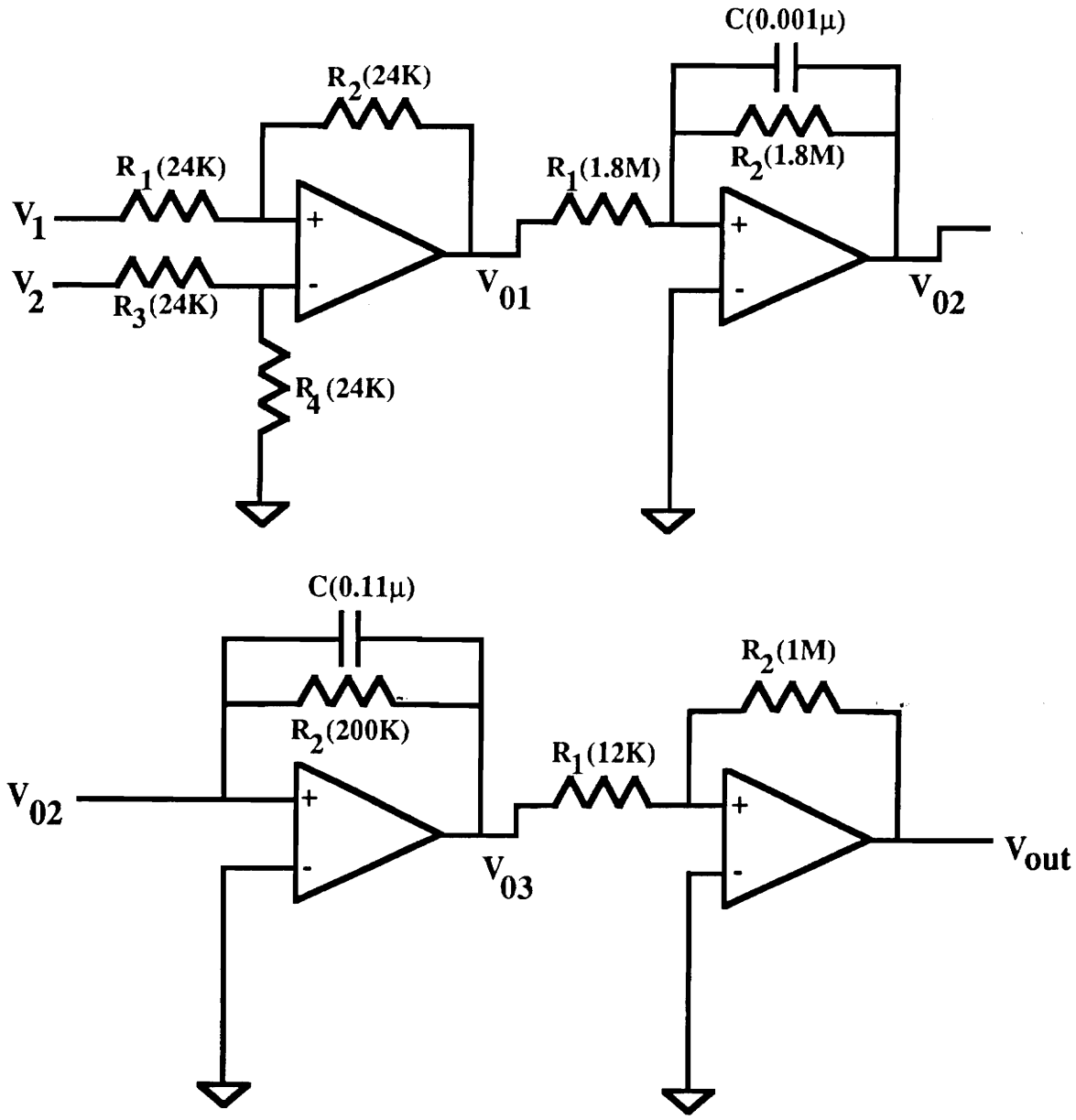

Figure 7. CIRCUIT DIAGRAM OF FEEDBACK CIRCUIT

$$V_{o1} = \frac{R_2}{R_1}(V_1 - V_2), \tag{5.2}$$

if $\frac{R_2}{R_1} = \frac{R_4}{R_3}$. As $R_1 = R_2 = R_3 = R_4$ the differential amplifier only subtracts the value of its two inputs to yield

$$V_{o1} = V_1 - V_2. \tag{5.3}$$

Substituting Eq. 5.1 in 5.3 the output of the differential amplifier is

$$V_{o1} = V_0 \cos \phi, \tag{5.4}$$

where $2V_B$ has been replaced by V_0.

The circuit diagrams of the low pass filter and the integrator are identical with only different component values. Fig. 8 shows a similar generic circuit and its Bode plot is shown in Fig. 9.

From the magnitude plot it can be seen that input signals are amplified depending on the ratio $\frac{R_2}{R_1}$ up to a frequency given by

$$f = \frac{1}{2\pi R_2 C}, \tag{5.5}$$

while signals above this frequency are attenuated at the rate of 20 dB/decade.

Also from the phase plot it can be seen that input signals above ten times the same frequency f given by Eq. 5.5 have a phase shift of 90° or $\pi/2$ radians at the output while signals below this frequency have a phase difference between 0 and $\pi/2$ radians between input and output. In all cases the output lags the input.

With this brief diversion the application of the above described circuit as a low pass filter and integrator is now discussed. For the low pass filter, on substituting individual component val-

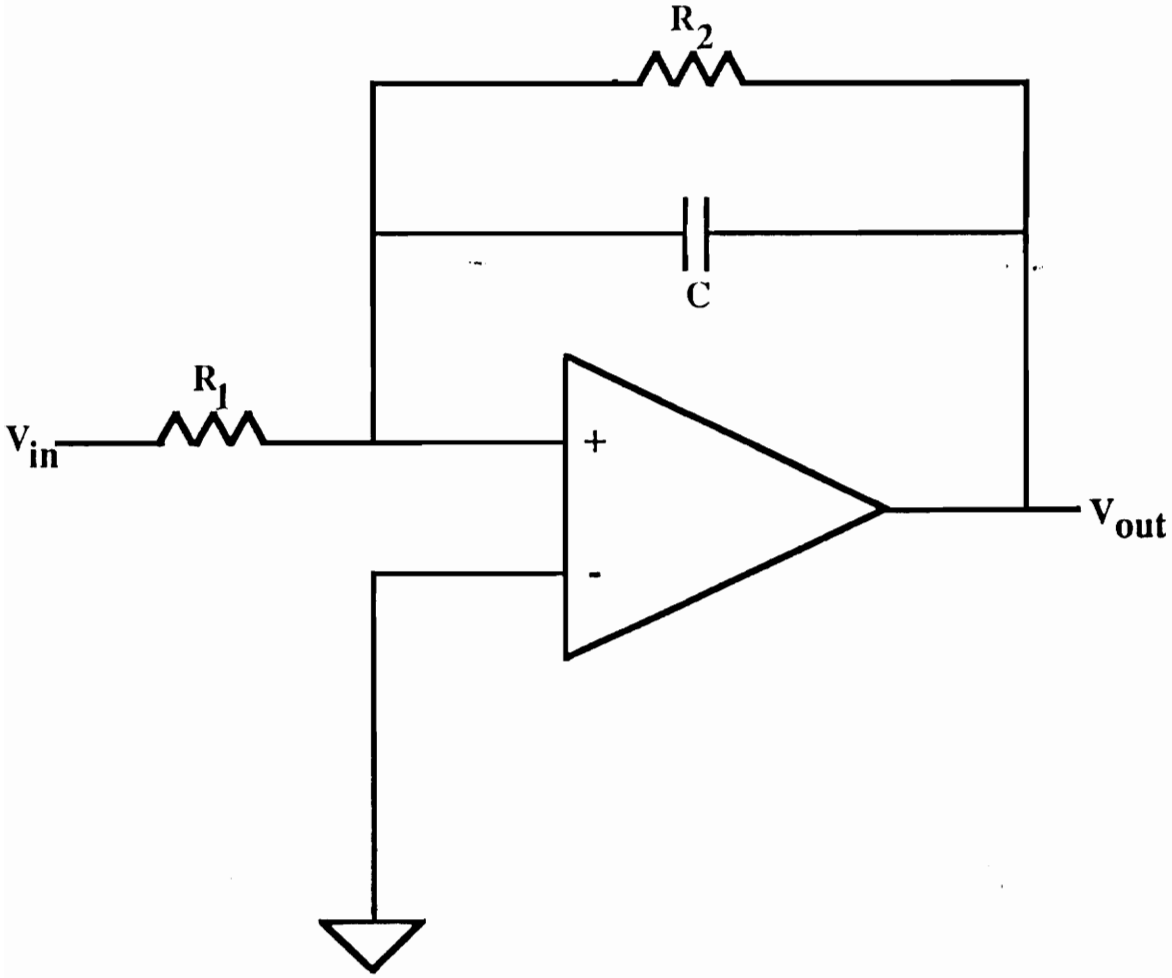

Figure 8. CIRCUIT DIAGRAM OF A LOW PASS FILTER OR INTEGRATOR

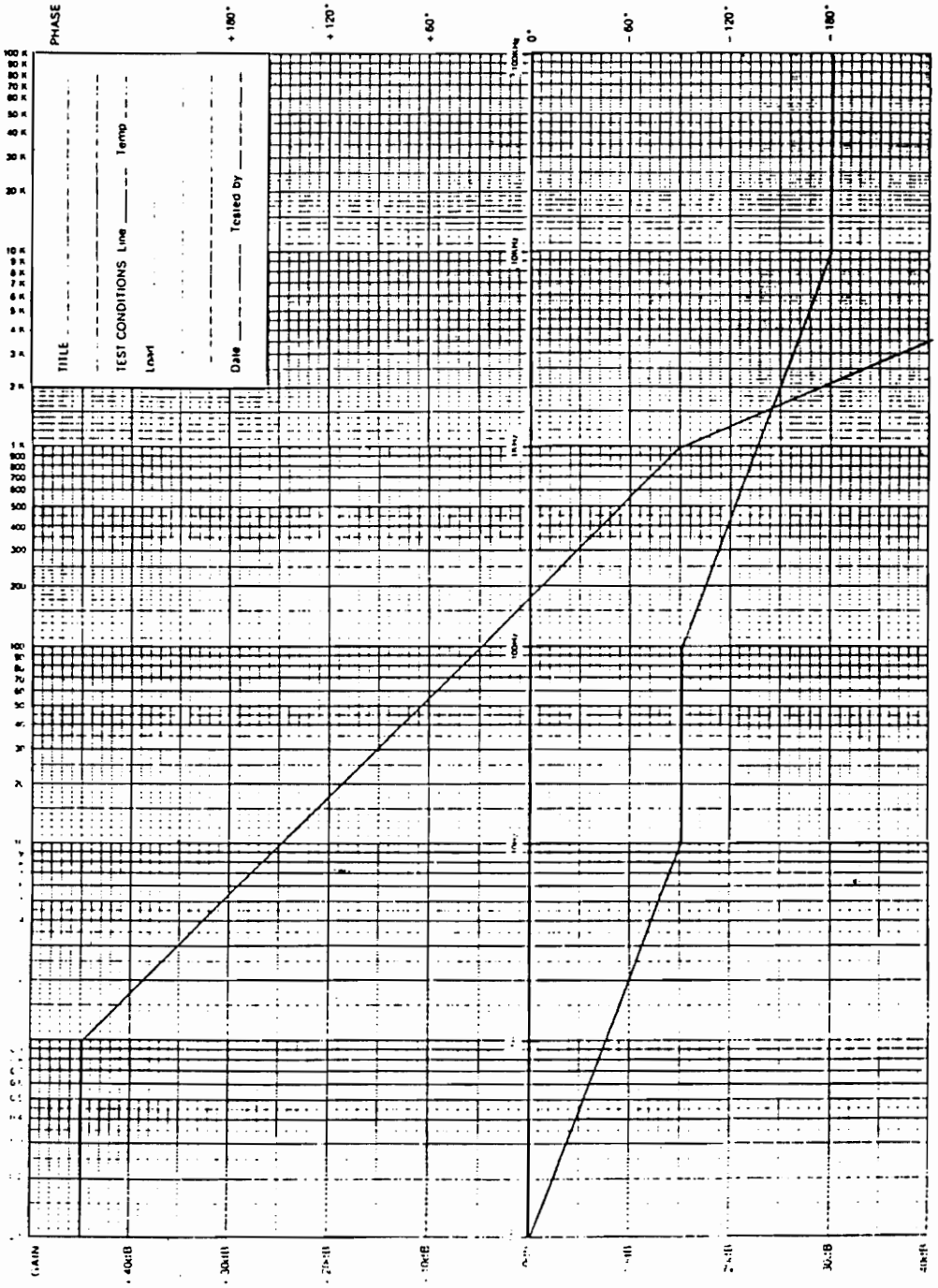

Figure 9. BODE PLOT OF A LOW PASS FILTER OR INTEGRATOR

ues into Eq. 5.5 it can be seen that input signals up to about 90 Hz. are passed with no attenuation (or amplification as $R_1 = R_2$) while signals above 90 Hz. are attenuated. There is also not much phase difference between the input and output signals up to about 40 Hz. Thus the output V_{o2} of the low pass filter is an exact reproduction of the input signal V_{o1} up to about 40 Hz. while signals between 40 and 90 Hz. vary in phase and signals above 90 Hz. are attenuated and shifted in phase by $\pi/4$ radians. Therefore V_{o2} can be described by

$$V_{o2} = V_{o1} = V_0 \cos \phi \tag{5.6}$$

up to about 40 Hz.

As an integrator it can be calculated by substituting component values into Eq. 5.5 that all input signals above 7 Hz. suffer a phase lag of $\pi/2$ radians at the output. Signals below about 3 Hz. do not have any appreciable phase change while signals between 3 and 7 Hz. have phase shifts in between $\pi/4$ and $\pi/2$ radians. Thus the circuit acts as an integrator for input signals above about 5 Hz. This part of the circuit has a small gain associated with it.

To get an overall picture, the output of the integrator is

$$V_{o3} = \int V_{o2} = V_0 \sin \phi \tag{5.7}$$

for signals between 5 and 40 Hz. Temperature and low frequency vibration noises exist in this frequency range. The output of the integrator is amplified and applied to the PZT element. The component values of the inverting amplifier are selected such that the output does not saturate while at the same time is close to the supply voltage of 15 volts.

In the general case, the range of frequencies compensated for is dictated by the individual component values of the low pass filter and the integrator. The low pass filter decides the upper limit of the the frequency range while the integrator decides its lower limit. Both are controlled by Eq. 5.5.

The PZT controls the length of the reference arm of the interferometer as a number of turns of fiber are wrapped around it. It thus controls the optical path-length difference and so the phase difference between the two arms as an expansion in its diameter increases the path length of the reference arm. As the optical phase between the two arms vary because of environmental noise the detector outputs vary as the cosine of this variation. The output of the feedback circuit follows this variation but with a phase lag of $\pi/2$ radians, i.e as the sine of the optical phase variation. This output when applied to the PZT controls the length of the reference arm and thus optical phase such that the optical phase difference between the arms of the interferometer is always $\pi/2$ radians or its odd multiple. This means that the interferometer is continuously held at quadrature.

5.3 MODES OF OPERATION

There are two modes of operation of the interferometer stabilized by the PZT method. They differ only in the frequency at which the signal of interest occurs and the upper limit of the cut-off frequency of the feedback loop. The discussion pertaining to them are also valid for interferometers stabilized by varying the source wavelength explained in section 4.3.1.

5.3.1 LOW GAIN MODE

The low gain mode of operation is useful for measuring phase variations of signals which are at a frequency higher than the cut off of the feedback loop. As explained in the previous section there is a low pass filter present in the feedback loop which decides the upper limit of the signals which have to be compensated for. In the low gain mode of operation the perturbation of interest which modulates the sensing arm of the interferometer occurs at a frequency much

higher than environmental noise. So the feedback loop compensates only for noise signals, i.e the low pass filter blocks all signals pertaining to the perturbation of interest. The output for the interferometer therefore is taken before the low pass filter, preferably at the output of the differential interferometer though it could be taken at the output of the detector itself. However taking the output after the differential amplifier reduces the effects of laser amplitude noise [14].

A band pass filter like the one shown in Fig. 10 can be applied at the output so that it passes the signal only in the frequency of interest and blocking signals at all the other frequencies. On determining the noise at that frequency the value of the minimum detectable signal can be calculated. The band pass filter is described in appendix B.

5.3.2 HIGH GAIN MODE

This mode of operation is useful for measuring signals which are at a frequency lower than the cut off frequency of the feedback loop, i.e the cut off frequency of the low pass filter is higher than the frequency at which the signal of interest occurs. For this mode of operation the output is taken at the output of the feedback circuit after the inverting amplifier. The high gain system has the has the advantage of greater dynamic range, less harmonic distortion and relative insensitivity to changes in laser output and coupler-splitting ratio [9].

Similar to the low gain mode the application of a band pass filter appropriately tuned cuts out the noise at other frequencies (see appendix B). The minimum detectable signal can again be calculated by finding out the value of noise at the frequency of interest.

The PZT method cannot be operated in the high gain mode when the signal of interest is at a frequency greater than 10 kHz. as the upper frequency response limit of a PZT cylinder is limited because of its circumferential resonance [9]. Even the method where the diode laser

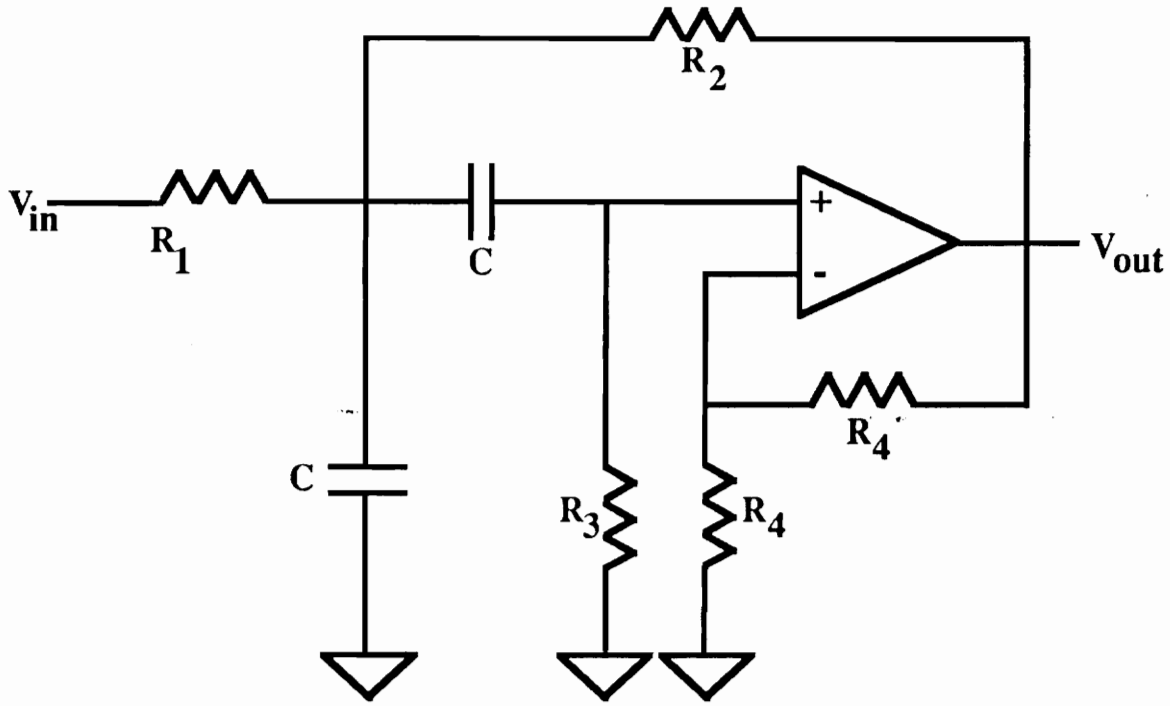

Figure 10. CIRCUIT DIAGRAM OF BAND PASS FILTER [15]

output frequency is tuned by its drive current cannot be operated in the high gain mode for very large modulation frequencies as indicated by Fig. 5 and Eq. 4.40.

5.4 RESULTS AND DISCUSSION

This section presents the results obtained on application of the PZT method of quadrature point stabilization on a Mach Zehnder interferometer configured as a magnetometer. The sensing arm was bonded to metglas and magnetic signals of known field amplitudes were applied using a solenoid. Since metglas responds to magnetic signals, the resulting changes in the length of metglas translates into variations in the phase difference between the arms of the interferometer. Comparisons are made between outputs plots obtained with and without the application of the stabilization.

Fig. 11 shows output fringes (see appendix A) when the sensing arm is modulated at 1 kHz and the interferometer is stabilized. This is the low gain mode of operation of the interferometer as the signal of interest is at 1 kHz, while the effects of noise perturbations are compensated for between 5 and 40 Hz. Without stabilization the output fringes displayed considerable signal fading. These effects could not be captured by the plotter at any instant as the signal fades and becomes large at a frequency equal to the noise frequency; instead a continuous time observation is required to see the deleterious effects of signal fading.

Figs. 12 and 13 display the output when the sensing arm is modulated at 10.4 Hz. The plot of Fig. 12 is taken without any stabilization enforced while Fig. 13 is taken from the stabilized interferometer. This is the high gain mode of operation of the interferometer as the signal of interest occurs at a frequency which lies in the frequency range for which the interferometer is compensated. Fig. 12 displays a unstable fringe pattern, though the instability of the signal

could not be captured on the plotter. Fig. 13 shows no fringes as the modulation of the sensing arm due to the applied magnetic field is compensated, in addition to all the low frequency noise perturbations.

So, in the time domain an interferometer without compensation produces output signals which are unstable and signal fading is observed. The application of quadrature point stabilization optimizes and stabilizes the output when the interferometer is operated in either the low or the high modes. The traces in Figs. 11, 12 and 13 were taken before the low pass filter, i.e at the output of the differential amplifier.

Fig. 14 displays the FFT of the feedback signal (passed through the band pass filter) taken without any modulation of the sensing arm. The interferometer is stabilized; it compensates for the effects of noise perturbations. Thus Fig. 14 shows the frequency distribution of environmental noise effects around 10 Hz. Finally Fig. 15 displays the FFT of the feedback signal when the sensing arm is modulated at 10.4 Hz and the interferometer is stabilized; it shows the frequency distribution of the magnetic signal and noise perturbations centered around 10 Hz. The signal to noise ratio can be determined from Figs. 14 and 15. The amplitude of the magnetic field which produced the trace in Fig. 15 can be calculated from the current applied to the coil [2]. The minimum detectable magnetic field can then be calculated for a signal to noise ratio (SNR) of 1.

The interferometer was stabilized for about 3 minutes after which the feedback system would saturate. This was due to the occurrence of a large noise signal and would result in the whole system moving to the next quadrature point (almost instantaneously) where the system would again be stabilized. Better thermal insulation of the whole set-up can considerably increase the period of time for which the interferometer is stabilized.

From Figs. 14 and 15 it can be determined that the SNR is slightly greater than 1000. The signal corresponds to a phase shift of approximately π radians. This results in a minimum detectable

phase shift of 10^{-3} radians. However, it can be observed from Fig. 15 that the minimum noise floor corresponds to about -95 dB which translates into a SNR of about 10^6, i.e theoretically, a minimum detectable phase shift of 10^{-6} radians can be obtained. To actually obtain this value of detectable phase shifts the noise floor at 10.4 Hz would have to be lowered from -66.7 to about -95 dB, though, only at 10.4 Hz. This can be achieved by reducing the flow of air around the set-up by properly enclosing it, by using better components and by using signal processing techniques to reduce the noise introduced by different electronic components and equipments.

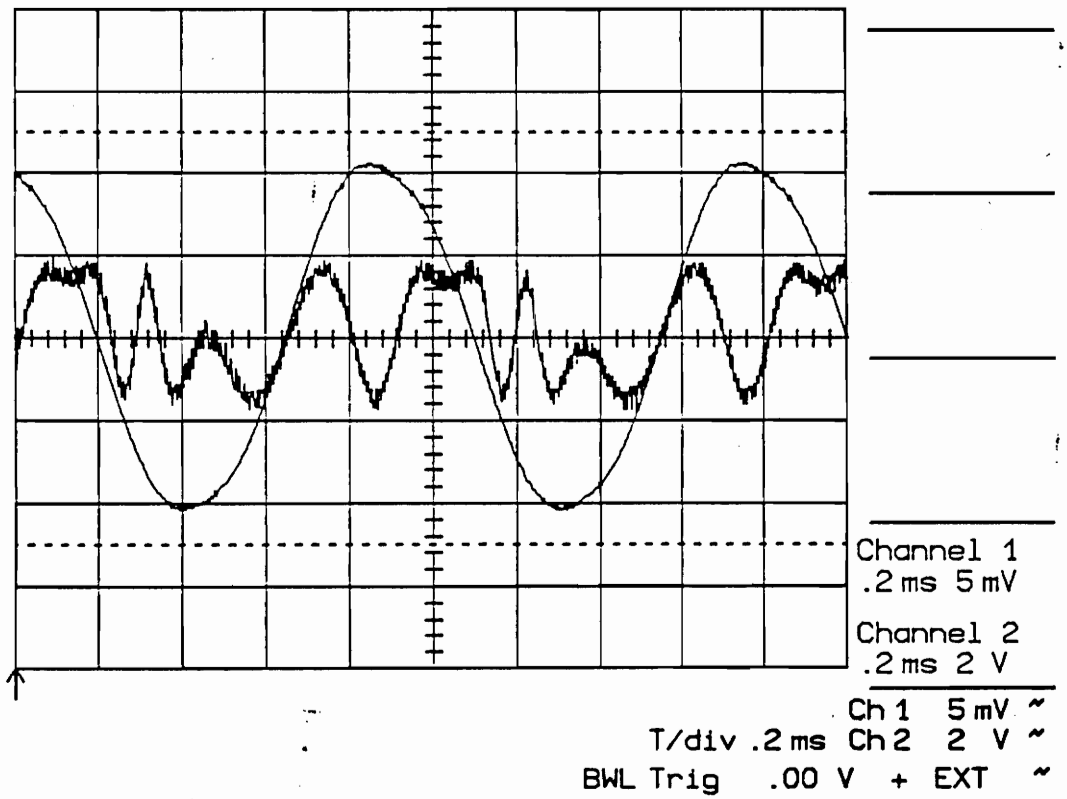

Figure 11. MODULATION AT 1 kHz. WITH STABILIZATION

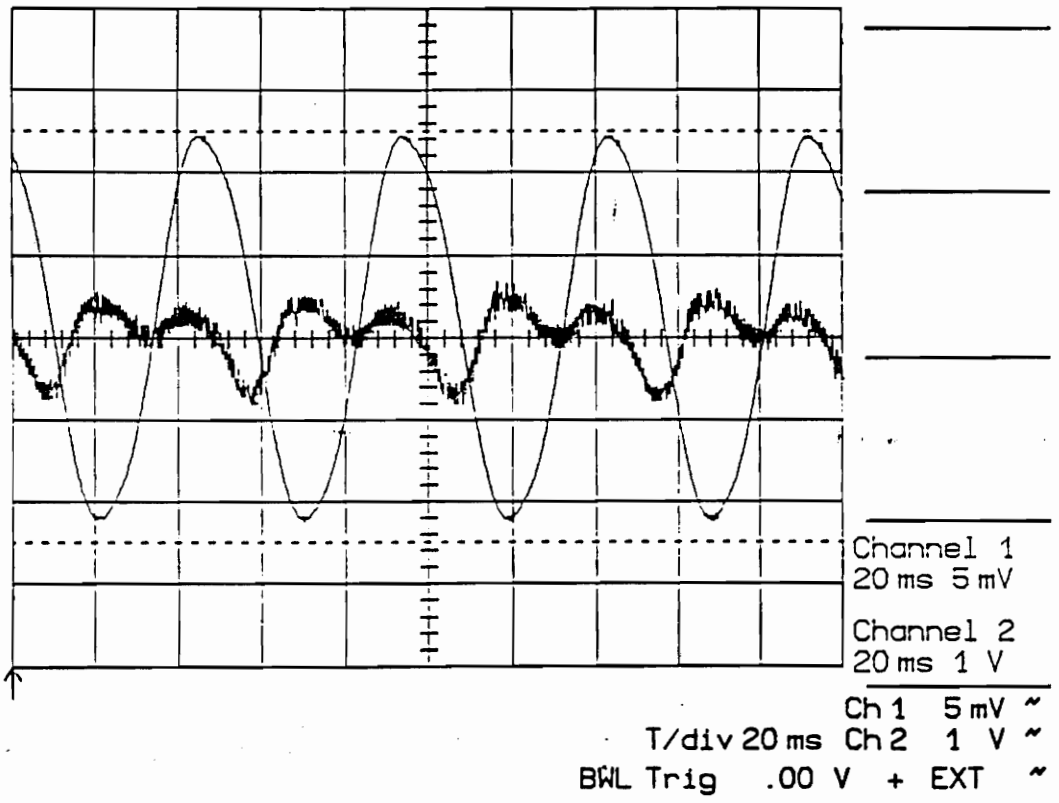

Figure 12. MODULATION AT 10 Hz. WITHOUT STABILIZATION

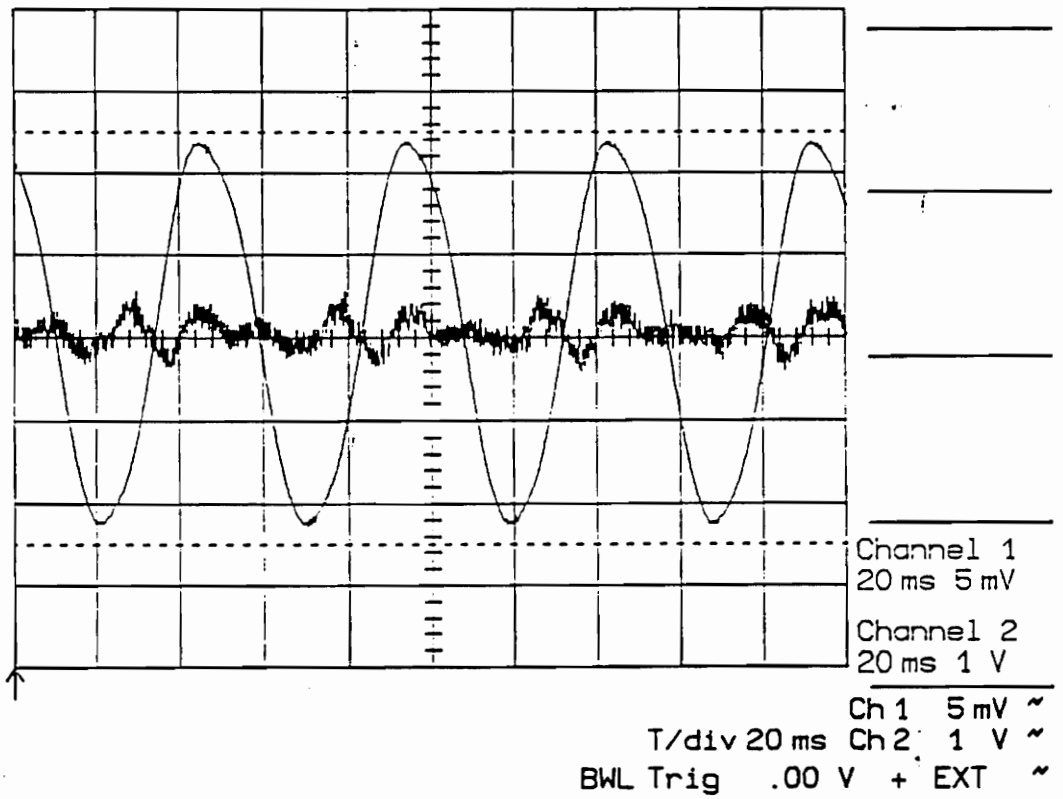

Figure 13. MODULATION AT 10 Hz. WITH STABILIZATION

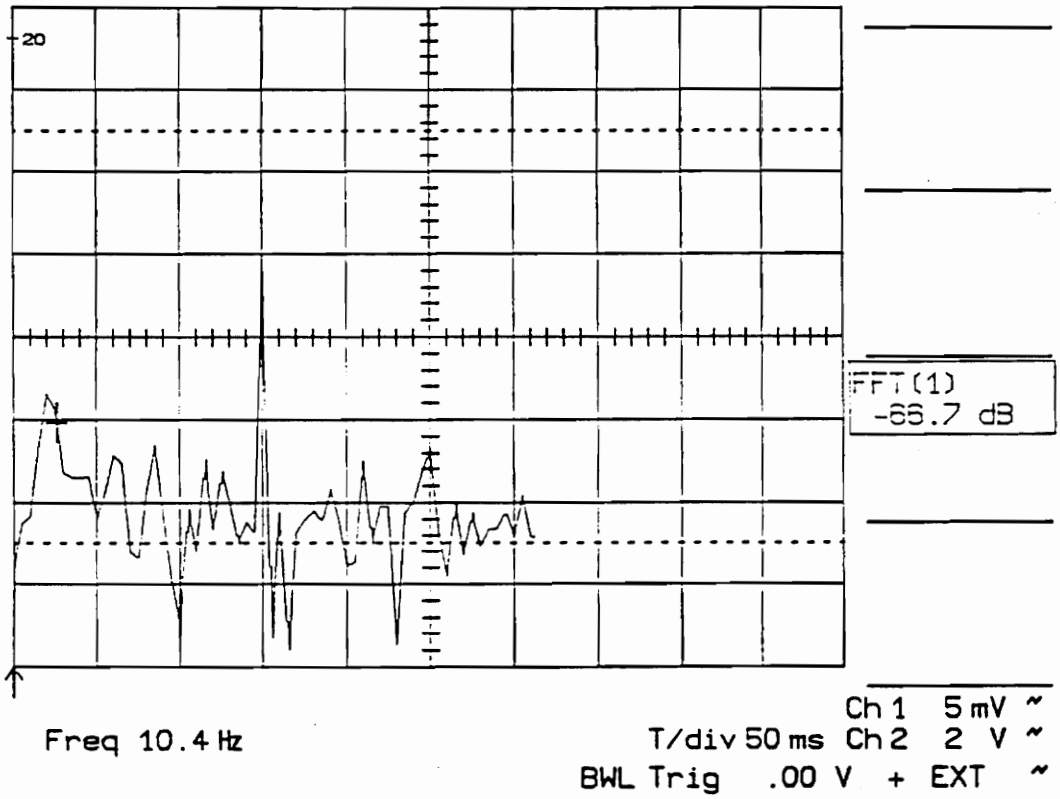

Figure 14. FFT OF FEEDBACK SIGNAL WITHOUT MODULATION

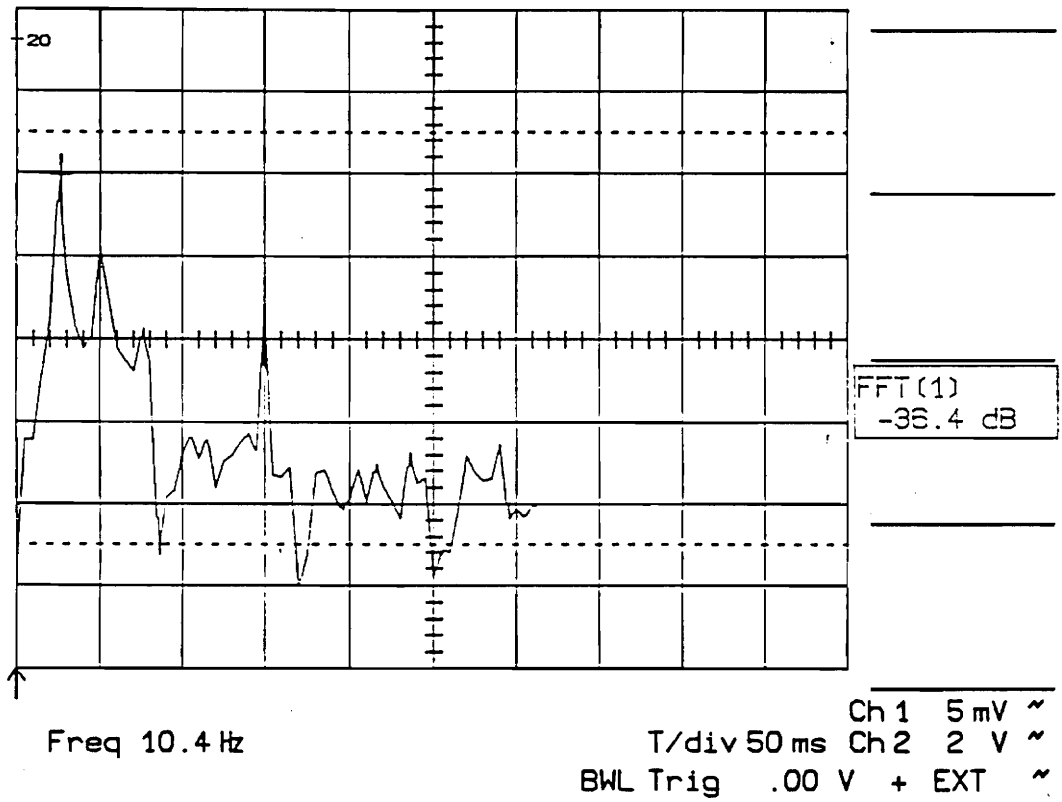

Figure 15. FFT OF FEEDBACK SIGNAL WITH MODULATION

6.0 CLOSING REMARKS

6.1 SUMMARY

A detailed explanation of the problem of signal fading present in interferometers in general has been provided. Different techniques to overcome this problem either actively or passively have been described.

A simple quadrature point stabilization circuit has been designed. Improved interferometer performance with a minimum detectable phase shift of 10^{-3} radians has been demonstrated. Methods to lower this floor to 10^{-6} radians have also been reviewed. Finally, for different frequency ranges where stabilization is required, the mathematical equations necessary for component value calculation have also been provided.

A review of the results for all the quadrature stabilization methods indicate that better minimum phase shifts can be detected with active methods rather than with passive methods [9]. While no results were provided for the Two Wavelength and Two Polarization Methods, application of the 3X3 coupler method resulted in a minimum detectable phase shift of 10^{-6}

radians for a 1 Hz signal processing bandwidth [10]. Both the active methods produced similar minimum detectable phase shifts in the micro-radian range [8, 9]. As described in the previous chapter these low values were calculated by considering the floor to which the noise could theoretically be lowered.

Appendix A. FRINGE PATTERN

When the perturbation of interest modulates the sensing arm of the Mach-Zehnder interferometer it translates into a modulation of the phase difference between the arms. If this modulation is not compensated for (low gain mode of operation), then a fringe pattern will be observed at the output of the detectors. The number of fringes at the output depends on the strength of the external field.

A simple computer program generates the data for the fringes which when plotted displays the formation of fringes as a function of the phase difference between the two arms.

A.1 PROGRAM TO GENERATE FRINGE PATTERN

```
program fringe (output); {* Pascal *}
const
   pi = 3.1412;
   a = 10; {* max value of phase difference *}
   i_in = 1; {* amplitude of output current *}
   max = 41; {* number of iterations *}
var
   i : integer;
   omegam_t_rad, {* phase difference in radians *}
   omegam_t_deg, {* phase difference in degrees *}
   i_out : real; {* output current *}
   outfile : text;
begin
   omegam_t_rad := 0;
   for i := 1 to max do
   begin
      i_out := i_in * (1 + cos (a * sin (omegam_t_rad)));
      omegam_t_deg := omegam_t_rad * 180 / pi; {* phase in degrees *}
      writeln (outfile, omegam_t_deg, i_out);
      omegam_t_rad := i * pi / 10; {* incrementing of phase *}
   end;
end.
```

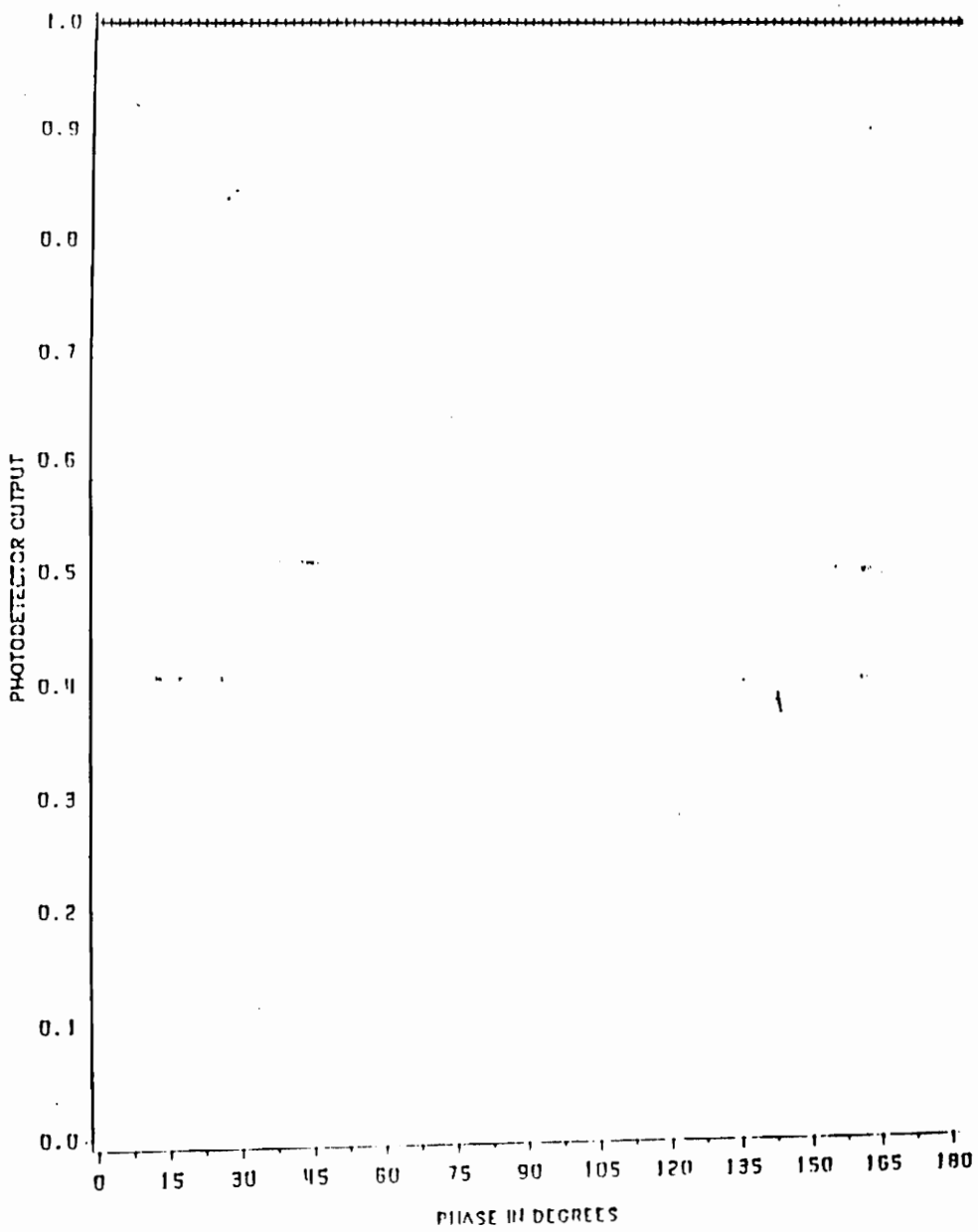

Figure 16. OUTPUT VERSUS PHASE DIFFERENCE (MAX = 0 RAD)

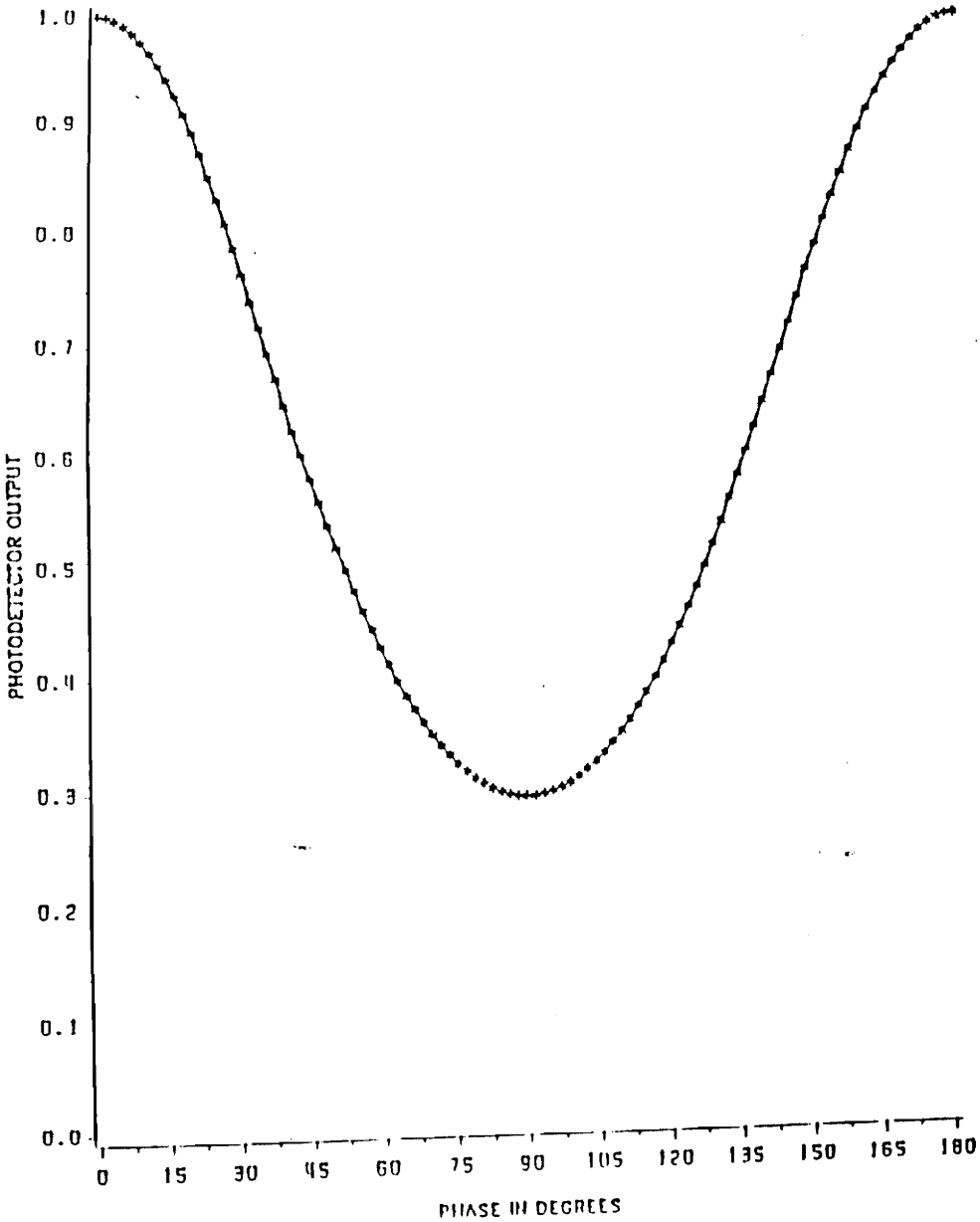

Figure 17. OUTPUT VERSUS PHASE DIFFERENCE (MAX = 2 RAD)

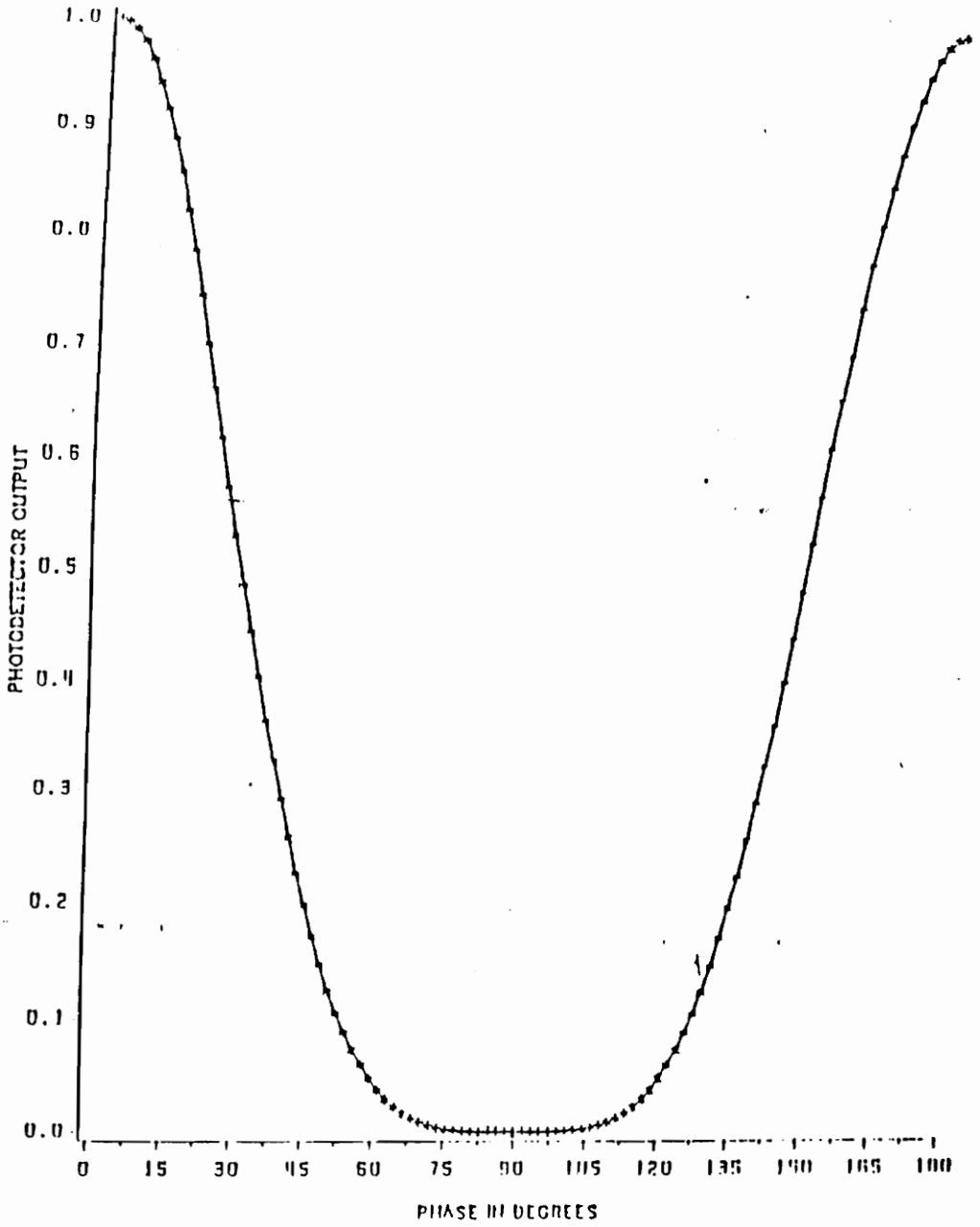

Figure 18. OUTPUT VERSUS PHASE DIFFERENCE (MAX = 3.14 RAD)

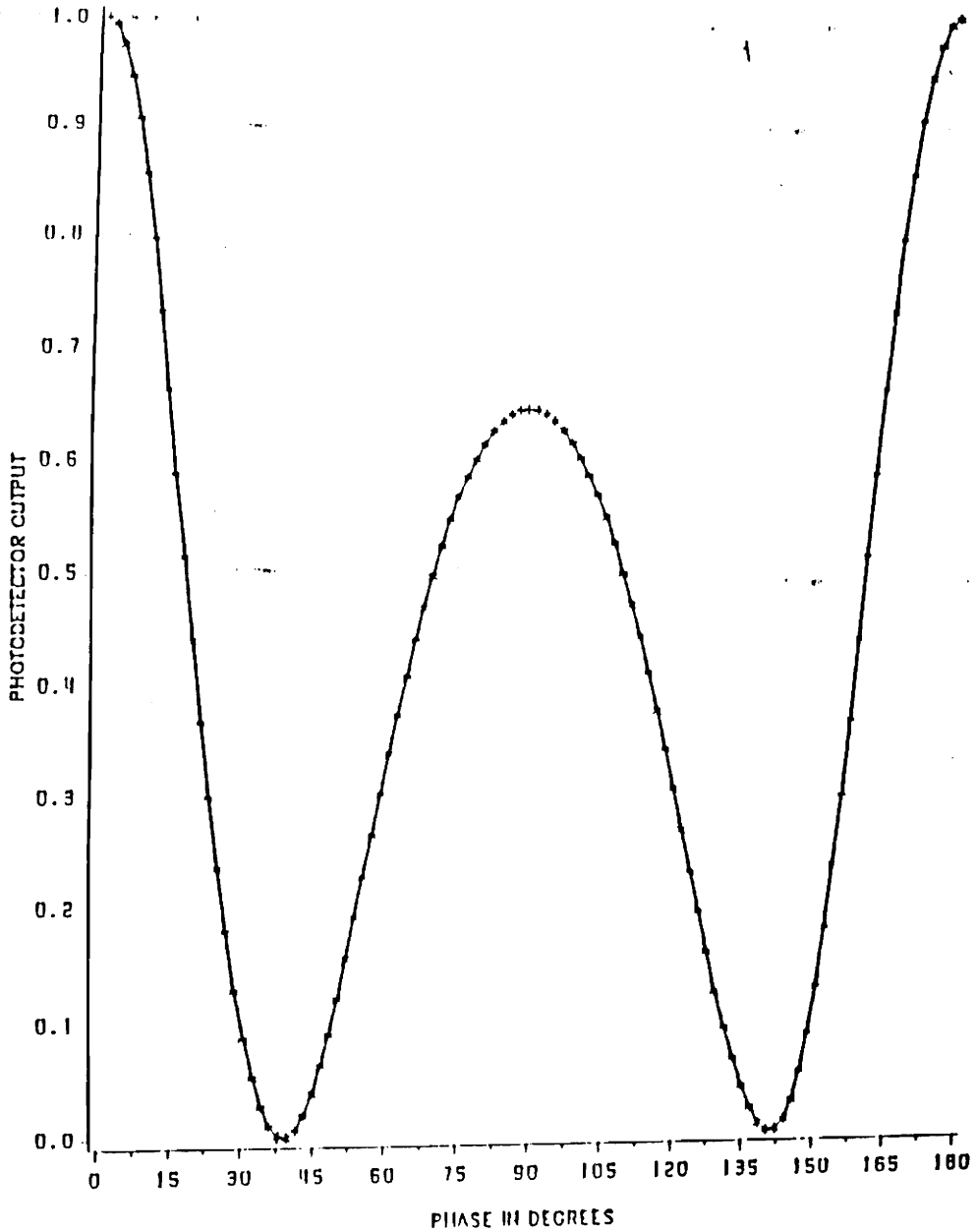

Figure 19. OUTPUT VERSUS PHASE DIFFERENCE (MAX = 5 RAD)

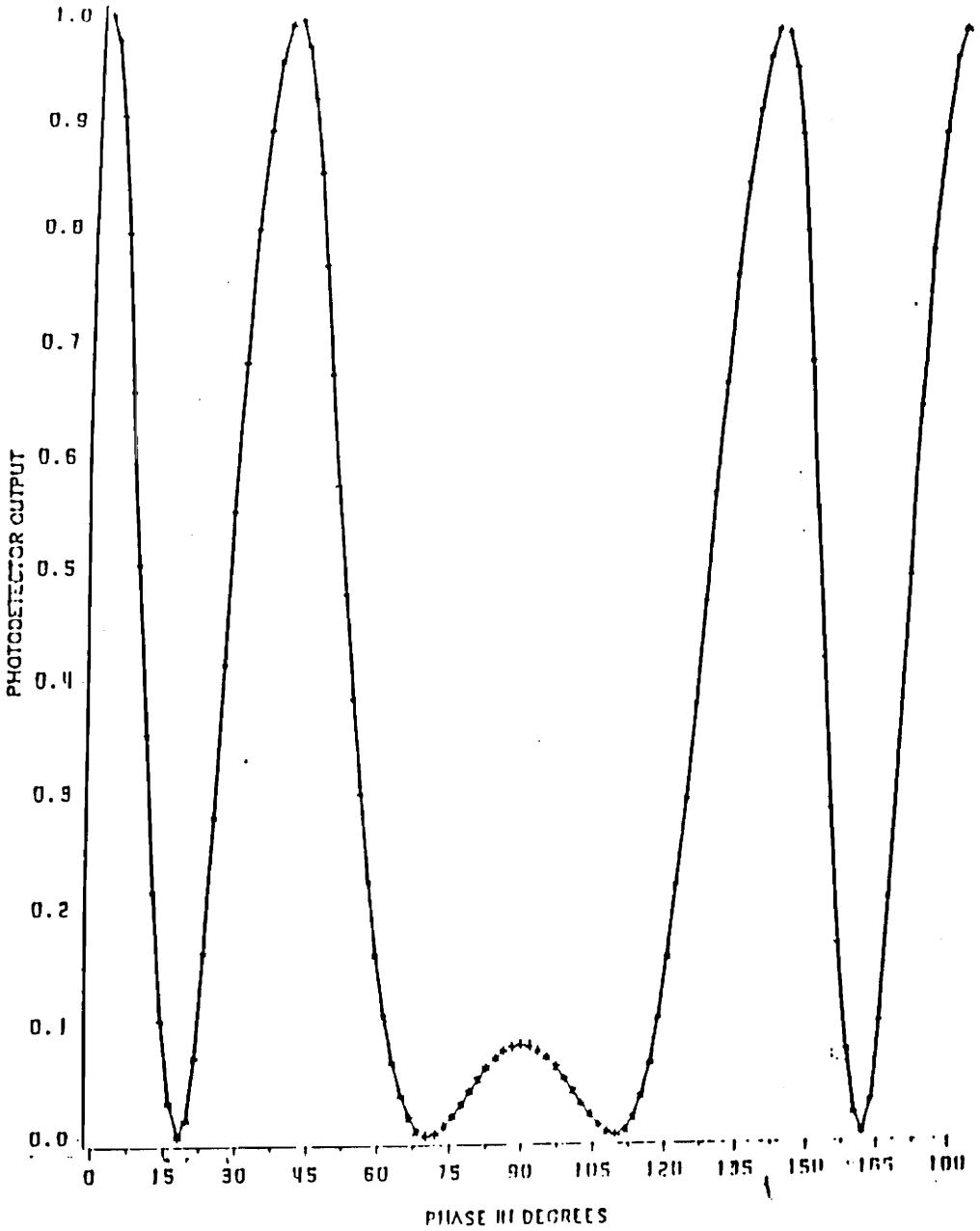

Figure 20. OUTPUT VERSUS PHASE DIFFERENCE (MAX = 10 RAD)

Appendix B. BAND PASS FILTER

A simple second-order band pass filter is given in Fig. 10 while the ideal and practical pass band magnitudes are given in Fig. 21 [15].

The bandwidth is given by

$$B = (\omega_U - \omega_L) radians/\sec , \tag{7.1}$$

or in hertz by

$$B = (f_U - f_L). \tag{7.2}$$

It is related to the quality factor Q by

$$Q = \frac{\omega_0}{B} , \tag{7.3}$$

or by

$$Q = \frac{f_0}{B} . \tag{7.4}$$

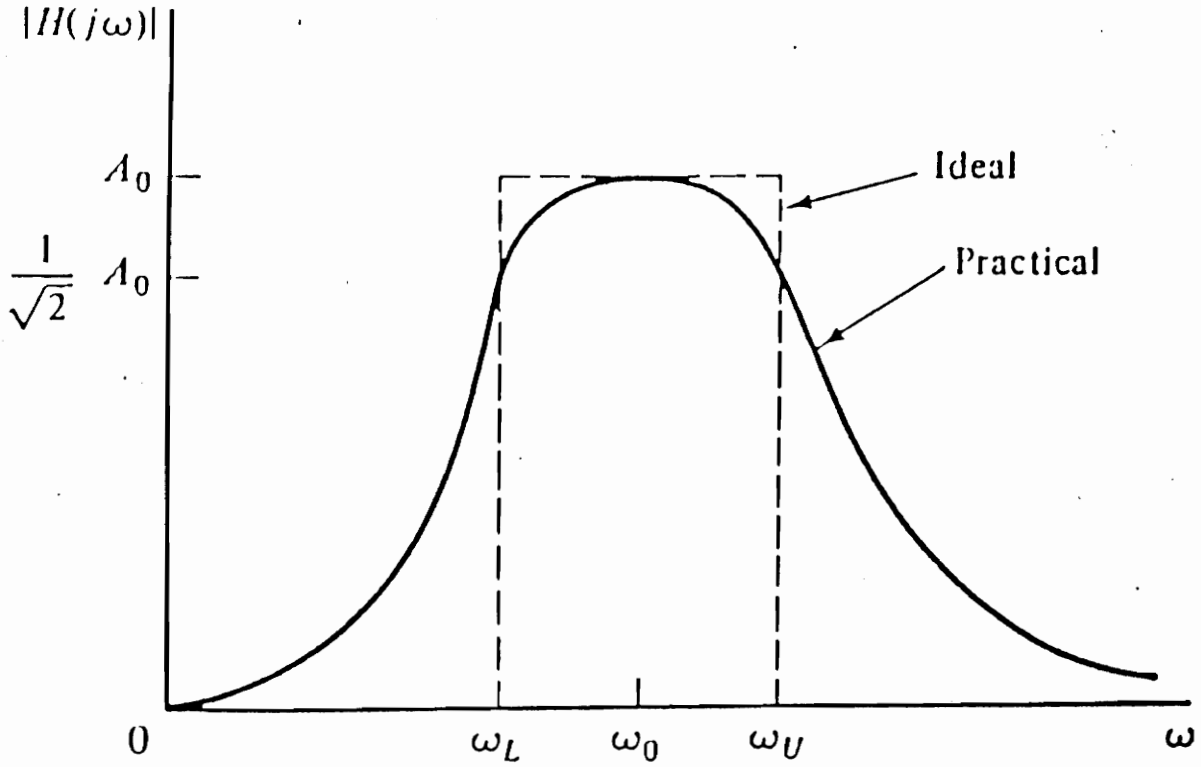

Figure 21. IDEAL AND PRACTICAL PASS BAND MAGNITUDES [15]

Thus, a high Q corresponds to a narrow bandwidth while a low Q corresponds to a wide bandwidth. For a second-order filter we have the following definitions which then help in calculation of component values.

$$\alpha = \frac{A_{BP}}{Q}, \tag{7.5}$$

where A_{BP} is the gain at the center frequency,

$$\beta = \frac{1}{Q}, \tag{7.6}$$

and,

$$\gamma = 1. \tag{7.7}$$

The resistor values in terms of the capacitance is then described by

$$R_1 = \frac{2}{\alpha\omega_0 C}, \tag{7.8}$$

$$R_2 = \frac{2}{[-\beta + \sqrt{(\alpha-\beta)^2 + 8\gamma}\,]\omega_0 C}, \tag{7.9}$$

$$R_3 = \frac{1}{\gamma\omega_0^2 C^2}\left(\frac{1}{R_1} + \frac{1}{R_2}\right), \tag{7.10}$$

and,

$$R_4 = 2R_3. \tag{7.11}$$

Substituting the component values in Fig. 10 into the equations it can be seen that the band pass filter is centered around 10 Hz. with a bandwidth of 1 Hz. and a gain of 1 at the center frequency.

BIBLIOGRAPHY

1. Culshaw B.; "Optical Fiber Sensing And Signal Processing", Peter Peregrinus Ltd., 1986

2. Nader N.; "Fiber Optic Interferometric Sensors", Thesis, Virginia Polytechnic Institute And State University, 1989

3. Bucholtz F., Koo K. P., Sigel G. H., Dandridge A.; "Optimization Of The Fiber/Metallic Glass Bond In Fiber-Optic Magnetic Sensors", J. Lightwave Tech., LT-3, No. 4, pp 814-817, 1985

4. Livingston J. D.; "Magnetomechanical Properties Of Amorphous Metals", Phys. Stat. Sol., Vol. 70, pp 591-596, 1982

5. Kersey A. D., Corke M., Jackson D. A., Jones J. D. C.; "Detection Of DC And Low-Frequency AC Magnetic Fields Using An All Single-Mode Fiber Magnetometer", Elect. Lett., Vol. 19, No. 13, pp 836-840, 1983

6. Kersey A. D., Jackson D. A., Corke M.; "Single-Mode Fiber-Optic Magnetometer With DC Bias Field Stabilization", J. Lightwave Tech., LT-3, No. 4, pp 836-840, 1985

7. Bucholtz F., Koo K. P., Kersey A. D., Dandridge A.; "Fiber Optic Magnetic Sensor Development", Proceedings Of The SPIE, Vol. 718, Fiber Optic And Laser Sensors IV, pp 56-65, 1986

8. Jackson D. A., Priest R. G., Dandridge A., Tveten A. B.; "Elimination Of Drift In A Single-Mode Optical Fiber Interferometer Using A Piezoelectrically Stretched Coiled Fiber", Appl. Opt., Vol. 19, No. 17, pp 2926-2929, 1980

9. Tveten A. B., Dandridge A.; "Phase Compensation In Interferometric Fiber-Optic Sensors", Opt. Lett., Vol.7, No. 6, pp 279-281, 1982

10. Koo K. P., Tveten A. B., Dandridge A.; "Passive Stabilization Scheme For Fiber Interferometers Using (3X3) Fiber Directional Couplers", Appl. Phys. Lett., Vol. 41, No. 7, pp 616-618, 1982

11. Sheem S. K.; Giallorenzi T. G., Koo K. P.; "Optical Techniques To Solve The Signal Fading Problem In Fiber Interferometers", Appl. Opt., Vol. 21, No. 4, pp 689-693, 1982

12. Shajenko P., Green E. L.; "Signal Stabilization Of Optical Interferometric Hydrophones By Tuning The Light Source", Appl. Opt., Vol. 19, No. 12, pp 1895-1897, 1980

13. Olsson A., Tang C. L., Green E. L.; "Active Stabilization Of A Michelson Interferometer By An Electrooptically Tuned Laser", Appl. Opt., Vol. 19, No. 12, pp 1897-1899, 1980

14. Dandridge A., Tveten A. B.; "Noise Reduction In Fiber-Optic Interferometer Systems", Appl. Opt., Vol. 20, No. 14, pp 2337-2339, 1981

15. Johnson D. E., Jayakumar V.; "Operational Amplifier Circuits: Design And Application", Prentice-Hall, Inc., 1982

Vita
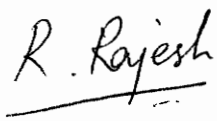
Rajesh Ramchander graduated from Osmania University, Hyderabad, India in June 1987 where he received his Bachelor of Engineering degree in Electrical Engineering with specialization in Instrumentation. Upon graduation he started graduate work and began research with Dr. R. O. Claus in the Fiber and Electro-Optics Research Center at Virginia Polytechnic Institute and State University. He is presently working towards a Masters degree in Computer Science and Applications at Virginia Tech.